Atmospheric
Chemistry
and Physics

Global modeling of aerosol nucleation with a semi-explicit chemical mechanism for highly oxygenated organic molecules (HOMs)

Xinyue Shao[1,2], Minghuai Wang[1,2], Xinyi Dong[1,2,3], Yaman Liu[1,4], Wenxiang Shen[1,2],
Stephen R. Arnold[5], Leighton A. Regayre[5,6,7], Meinrat O. Andreae[8,9], Mira L. Pöhlker[8,10,11],
Duseong S. Jo[12,a], Man Yue[1,4], and Ken S. Carslaw[5]

[1]School of Atmospheric Science, Nanjing University, Nanjing, 210023, China
[2]Joint International Research Laboratory of Atmospheric and Earth System Sciences & Institute for Climate
and Global Change Research, Nanjing University, Nanjing, 210023, China
[3]Frontiers Science Center for Critical Earth Material Cycling, Nanjing University, Nanjing, China
[4]Zhejiang Institute of Meteorological Sciences, Hangzhou, 310008, China
[5]Institute for Climate and Atmospheric Science, School of Earth and Environment,
University of Leeds, Leeds, LS2 9JT, UK
[6]Met Office Hadley Centre, Exeter, Fitzroy Road, Exeter, Devon, EX1 3PB, UK
[7]Centre for Environmental Modelling and Computation, School of Earth and Environment,
University of Leeds, Leeds, LS2 9JT, UK
[8]Max Planck Institute for Chemistry, 55020 Mainz, Germany
[9]Scripps Institution of Oceanography, University of California, San Diego, La Jolla, CA, USA
[10]Leipzig Institute for Meteorology, Universität Leipzig, 04103 Leipzig, Germany
[11]Experimental Aerosol and Cloud Microphysics Department, Leibniz Institute for Tropospheric Research,
04318 Leipzig, Germany
[12]Atmospheric Chemistry Observations and Modeling Laboratory, National Center for Atmospheric Research,
Boulder, CO 80103, USA
[a]now at: Department of Earth System Science Education, Seoul National University,
Seoul, 999 007, South Korea

Correspondence: Minghuai Wang (minghuai.wang@nju.edu.cn) and Xinyi Dong (dongxy@nju.edu.cn)

Abstract. New particle formation (NPF) involving organic compounds has been identified as an important process affecting aerosol particle number concentrations in the global atmosphere. Laboratory studies have shown that highly oxygenated organic molecules (HOMs) can make a substantial contribution to NPF, but there is a lack of global model studies of NPF with detailed HOM chemistry. Here, we incorporate a state-of-the-art biogenic HOM chemistry scheme with 96 chemical reactions to a global chemistry–climate model and quantify the contribution to global aerosols through HOM-driven NPF. The updated model captures the frequency of NPF events observed at continental surface sites (normalized mean bias changes from −96 % to −15 %) and shows reasonable agreement with measured rates of NPF and sub-20 nm particle growth. Sensitivity simulations show that compared to turning off the organic nucleation rate, turning off organic initial growth results in a more substantial decrease in aerosol number concentrations. Globally, organics contribute around 45 % of the annual mean vertically integrated nucleation rate (at 1.7 nm) and 25 % of the vertically averaged growth rate. The inclusion of HOM-related processes leads to a 39 % increase in the global annual mean aerosol number burden and a 33 % increase in cloud condensation nuclei (CCN) burden at 0.5 % supersaturation compared to a simulation with only inorganic nucleation. Our work predicts a greater contribution of organic nucleation to NPF than previous

studies due to the semi-explicit HOM mechanism and an updated inorganic NPF scheme. The large contribution of biogenic HOMs to NPF on a global scale could make aerosol sensitive to changes in biogenic emissions.

1 Introduction

Aerosols exert multifaceted impacts on both climate and human health across a range of environments (Wang and Penner, 2009; Rosenfeld et al., 2014; Shiraiwa et al., 2017; Bellouin et al., 2020; Carslaw, 2022; Rosenfeld et al., 2008). Atmospheric new particle formation (NPF) is a significant contributor to aerosol number concentration that involves the nucleation of stable molecular clusters via gas-to-particle conversion and their subsequent growth through the condensation of precursor vapors (Merikanto et al., 2009; Spracklen et al., 2010; Kerminen et al., 2018; Kulmala, 2003). While both the nucleation and growth of new particles are commonly linked to sulfuric acid (H_2SO_4) owing to its low volatility, H_2SO_4 and its inorganic clusters (e.g., H_2SO_4–NH_3 clusters) alone are insufficient to explain the rapid nucleation rates observed in forested regions minimally affected by anthropogenic pollution (Kuang et al., 2008; Sihto et al., 2006; Kerminen et al., 2018; Stolzenburg et al., 2020; Weber et al., 1997; Boy et al., 2008; Paasonen et al., 2010; Andreae et al., 2022). Furthermore, while H_2SO_4 frequently initiates cluster formation, its concentration does not account for the high growth rates of particles larger than 3 nm diameter (Ehn et al., 2014; Deng et al., 2020).

Laboratory studies and ambient measurements have shown that highly oxygenated organic molecules (HOMs) largely account for the particle nucleation and growth rate in forested areas, owing to their extremely low volatility. Riccobono et al. (2014) revealed a nucleation mechanism involving both H_2SO_4 and oxidized organic molecules from the very first step, and including this mechanism in a global aerosol model yielded a seasonal cycle of particle concentrations in the continental boundary layer, in good agreement with observations. Jokinen et al. (2015) found that monoterpene-derived HOMs promote NPF under continental conditions using chamber experiments. Kirkby et al. (2016) showed that the rate of formation of particles from biogenic HOMs, in the absence of H_2SO_4, can be enhanced by 1–2 orders of magnitude by ions based on CERN CLOUD (Organisation Européene pour la Recherche Nucléaire – Cosmics Leaving Outdoor Droplets) experiments. In addition to contributing to the formation of 1–2 nm clusters, Ehn et al. (2014) showed that HOMs made important contributions to the particle growth, with diameters between 5 and 50 nm in northern forests, which was recently explained by Mohr et al. (2019) at the molecular level. Bianchi et al. (2016) also showed observational evidence that NPF occurs mainly through condensation of HOMs at high altitude.

Although HOMs are necessary for NPF in the absence of H_2SO_4 (Kirkby et al., 2016), the molecular structures and formation pathways of HOMs remain uncertain and are treated in a variety of ways in models. Gordon et al. (2016) simulated monoterpene-derived HOM formation using an empirical or semiempirical fixed yield of HOMs from the first-stage monoterpene oxidation products, although with highly simplified HOM chemistry. Zhu et al. (2019) added some explicit chemical mechanisms for HOMs, but they did not consider autoxidation and used a less stringent definition of HOMs than recommended in Bianchi et al. (2019). Roldin et al. (2019) used a more explicit reaction mechanism to treat the generation of HOMs through autoxidation and cross-reactions of α-pinene oxidation products in a 1-D column model. Weber et al. (2020) used a similarly explicit mechanism over the boreal forest in Finland and the southeast USA, although not on a global scale.

There is thus a lack of global-scale simulations of NPF with explicit HOM chemistry and quantification of the contribution of organics to aerosol and CCN number concentrations. Recently, Xu et al. (2022) summarized the various chemical mechanisms of HOMs, including monoterpene-derived peroxy radical (MT-RO_2) unimolecular autoxidation and self- and cross-reactions with other RO_2 species, and evaluated them in the GEOS-Chem global model. However, they did not quantify the effects of HOMs participating in NPF. Here, we incorporate the representation of HOMs from Xu et al. (2022) within a global chemistry–climate model and then quantify the contribution of HOMs to aerosol number concentration globally. Inorganic nucleation rates involving H_2SO_4 and NH_3 as well as ion-induced pathways based on the CLOUD chamber experiments are also included (Dunne et al., 2016), replacing a simpler scheme based on H_2SO_4 and NH_3 (Vehkamaki et al., 2002; Merikanto et al., 2007).

The model and field measurements used in this study are documented in Sect. 2. Section 2.6 evaluates outputs of the updated model, including nucleation and growth rates, frequencies of NPF events, and aerosol number concentrations. Additionally, four sensitivity experiments aimed at investigating uncertainties in concentrations of organic nucleating species and disentangling the roles of nucleation and growth processes are conducted. Section 3 quantifies the contributions of organic-related processes to nucleation rate, growth rate, aerosol, and CCN number concentrations globally. Section 4 compares the proportion of the organic nucleation rate with previous studies. Results are summarized and discussed in Sect. 5.

2 Data and methods

2.1 Model configuration

We use the atmospheric component of the Community Earth System Model (CESM) version 2.1.0, the Community Atmosphere Model version 6, augmented with comprehensive tropospheric and stratospheric chemistry (CAM6-Chem) (Emmons et al., 2020). Biogenic emissions are dynamically simulated using the Model of Emissions of Gases and Aerosol from Nature version 2.1 (MEGAN2.1) (Guenther et al., 2012). We use the historical anthropogenic emissions developed by the Community Emission Data System (CEDS v2017-05-18) in support of phase 6 of the Coupled Model Intercomparison Project (CMIP6) (Hoesly et al., 2018). Monthly biomass burning emissions are from the historical global biomass burning emissions inventory for CMIP6 (van Marle et al., 2017). Emissions for the 1997 to 2015 period in this inventory have been derived from satellite-based emissions from the Global Fire Emissions Database (van der Werf et al., 2017). The vertical distribution of biomass burning emissions is taken from Dentener et al. (2006). All the emission data can be downloaded from https://svn-ccsm-inputdata.cgd.ucar.edu/trunk/inputdata/atm/cam/chem/emis/ (last access: 3 October 2024). The previous study (Paulot et al., 2018) reported that there is an overestimation of SO_2 emissions over China after 2007 due to the underestimation of the SO_2 reduction. Therefore, emissions in China were replaced by the Multi-resolution Emission Inventory for China (MEIC) (http://www.meicmodel.org, last access: 3 October 2024) (Li et al., 2017; Yue et al., 2023), which considerably improves Chinese emission inventories, compared to the earlier large-scale studies (Zheng et al., 2009; Zhou et al., 2017). CAM6-Chem utilizes a four-mode version of the Modal Aerosol Module (MAM4) (Liu et al., 2016), coupled with the Model for Simulating Aerosol Interactions and Chemistry (MOSAIC) (Zaveri et al., 2021), to explicitly represent the heterogeneous uptake of isoprene epoxydiols (IEPOX) onto sulfate aerosols and their subsequent production (Jo et al., 2019; 2021). Following Liu et al. (2023), we adopt a modest photolysis rate for monoterpene-derived secondary organic aerosols, constituting 2.0 % of the NO_2 photolysis frequency (Bianchi et al., 2019; Krapf et al., 2016; Zawadowicz et al., 2020). All simulations were run at a horizontal resolution of 0.95° latitude and 1.25° longitude, with a vertical resolution extending up to approximately 40 km across 32 layers (Emmons et al., 2020). To follow the observed meteorological conditions and initialize realistic meteorological conditions, meteorological fields (temperature and wind profiles, surface pressure, surface stress, surface heat, and moisture fluxes) are nudged toward Modern-Era Retrospective analysis for Research and Applications (MERRA2) reanalysis (Kooperman et al., 2012), which allows model–observation comparisons that are unaffected by variability in synoptic-scale model dynamics. We evaluate model performance against observations from multiple years (Sect. 2.6), where in each case the anthropogenic emissions and model meteorology correspond to values associated with the observation year.

We incorporate advanced chemical reactions involving the formation of HOMs, since in the default configuration of CAM6-Chem, organics are not involved in either the nucleation or the initial growth processes of aerosols (sub-20 nm). These include MT-RO_2 unimolecular H shifts (i.e., "autoxidation") and self- and cross-reactions with other RO_2 species, guided by laboratory-derived mechanistic parameters from Xu et al. (2022). In total, 24 reactions in CAM6-Chem were modified and 96 reactions were added. Descriptions of chemical mechanisms are shown in Sect. S1 in the Supplement, and the final products, including HOMs and accretion products (ACC, C15, and C20), are summarized in Table 1.

2.2 Nucleation and growth scheme in CAM6-Chem

2.2.1 Nucleation scheme in default CAM6-Chem

The default configuration of CAM6-Chem (Default; Table 2) includes binary homogeneous nucleation of H_2SO_4–H_2O (Vehkamaki et al., 2002) and ternary homogeneous nucleation of H_2SO_4–NH_3–H_2O (Merikanto et al., 2007). Additionally, within the boundary layer the model includes the empirical mechanism of Kulmala et al. (2006) and Sihto et al. (2006), as first used in a global model by Spracklen et al. (2006):

$$j_{1\,nm} = A[H_2SO_4], \tag{1}$$

where A ($1.0^{-6}\,s^{-1}$) is the rate constant chosen from the median values derived in case studies (Sihto et al., 2006).

2.2.2 Updated inorganic nucleation scheme

Most existing models tend to overestimate the sensitivity of the nucleation rate to sulfuric acid concentrations when relying solely on classical nucleation theories of sulfuric acid (Ehn et al., 2014; Mann et al., 2014; Scott et al., 2014). Therefore our study updates the inorganic nucleation parameterizations in CAM6-Chem, drawing upon data from the CLOUD chamber experiments (Kirkby et al., 2016; Dunne et al., 2016). The updated schemes incorporate H_2SO_4, NH_3 and ions. The inorganic NPF rates at a mobility equivalent diameter of 1.7 nm are calculated by summing the following rates (Dunne et al., 2016).

The nucleation rate of binary neutral (indicated by b, n, J_{SA}) and ion-induced (b, i, $J_{SA,i}$) involving sulfuric acid and water is calculated using Eqs. (2) and (3).

$$J_{SA} = K_{b,n}(T)[H_2SO_4]^{P_{b,n}} \tag{2}$$

$$J_{SA,i} = K_{b,i}(T)[H_2SO_4]^{P_{b,i}}[n-], \tag{3}$$

Table 1. The molecular formula, saturated vapor concentration (C^*) at 300 K, enthalpy of vaporization (ΔH_{vap}), and corresponding volatility class of newly added organics.

Species	Short name	Molecular formula	$\log(C^*)$ ($\mu g\,m^{-3}$)	ΔH_{vap} ($kJ\,mol^{-1}$)	Volatility bin[a]
HOMs	C10-NON[b]	$C_{10}H_{14}O_9$	-3.22	164.0	LVOC
	C10-ON[c]	$C_{10}H_{14}O_9N$	-3.31	164.0	LVOC
ACC[d]	C15	$C_{15}H_{18}O_9$	-5.20	186.0	ELVOC
	C20	$C_{20}H_{32}O_8$	-9.53	230.0	ULVOC

[a] LVOCs, ELVOCs, and ULVOCs represent low-volatility, extremely low volatility, and ultra-low-volatility organic compounds, respectively. [b] NON represents non-organonitrates. [c] ON represents organonitrates. [d] ACC represents accretion products.

Table 2. Configurations of CESM2.1.0 experiments.

Test name	Updated inorganic nucleation	HOM chemistry	Organic nucleation	Organic growth	Other changes
Default	×	×	×	×	–
Inorg	✓	✓	×	×	–
Inorg_Org	✓	✓	✓	✓	–
Only_NR	✓	✓	✓	×	–
Only_GR	✓	✓	✓	×	–
Low_Br	✓	✓	✓	✓	Lower branching ratio of the first-generation product (MT-RO$_2$) from MT + O$_3$ and MT + OH, which could be further auto-oxidized
Slow_NO	✓	✓	✓	✓	Rate of MT-HOM-RO$_2$ + NO generating HOMs, multiplied by 0.2
High_temp	✓	✓	✓	✓	Autoxidation rate with high temperature dependence (Roldin et al., 2019) (Table S8)
Low_temp					Autoxidation rate with low temperature dependence (Weber et al., 2020) (Table S8)
Fast_auto	✓	✓	✓	✓	Autoxidation rate multiplied by 10
Slow_auto	✓	✓	✓	✓	Autoxidation rate multiplied by 0.1
Slow_accr	✓	✓	✓	✓	Using slower self- and cross reaction rate derived from Weber et al. (2020) and Berndt et al. (2018) (Table S9)

where $K(T)$ denotes temperature-dependent prefactors, P_i denotes constant parameters, and $[n-]$ is the concentration of negative ions produced from galactic cosmic rays (equal to $[n\pm]$ in Eq. (8), which is parameterized in Sect. S2).

The nucleation rate of ternary neutral (indicated by t, n, J_{SA-NH_3}) and ion-induced (t, i, $J_{SA-NH_3,i}$) involving sulfuric acid, ammonia, and water is calculated using Eqs. (4) and (5).

$$J_{SA\text{-}NH_3} = K_{t,n}(T) f_n([NH_3], [H_2SO_4])[H_2SO_4]^{P_{t,n}} \quad (4)$$

$$J_{SA\text{-}NH_3,i} = K_{t,i}(T) f_i([NH_3], [H_2SO_4])[H_2SO_4]^{P_{t,i}}[n-], \quad (5)$$

where $f([NH_3], [H_2SO_4])$ denotes functions of the ammonia and sulfuric acid gas-phase concentrations, also involving free-fitting parameters.

2.2.3 New organic nucleation scheme

There is no organic nucleation scheme in the Default (Table 2), so organic NPF rates at a 1.7 nm mobility equivalent diameter were included as the sum of the following parameterizations.

The rate of heteromolecular nucleation of sulfuric acid and organics (HET; $J_{\text{SA-Org}}$) is parameterized following Riccobono et al. (2014), depending on both H_2SO_4 and organic nucleating species concentration:

$$J_{\text{SA-Org}} = K_m[H_2SO_4]^2[\text{HOM} + \text{ACC}], \tag{6}$$

where ACC represents accretion products (Table 1), and K_m is the multicomponent prefactor, which is equal to $3.27 \times 10^{-21} \text{ cm}^6 \text{ s}^{-1}$ (Riccobono et al., 2014).

The rates of neutral pure organic nucleation (NON; $J_{\text{Org,n}}$) and ion-induced pure organic nucleation (ION; $J_{\text{Org,i}}$) are parameterized based on Kirkby et al. (2016):

$$J_{\text{Org,n}} = a_1[\text{ACC}]^{a_2 + \frac{a_5}{[\text{ACC}]}} \tag{7}$$

$$J_{\text{Org,i}} = [n\pm]a_3[\text{ACC}]^{a_4 + \frac{a_5}{[\text{ACC}]}}, \tag{8}$$

where ACC is in units of $10^7 \text{ molec. cm}^{-3}$, a_n parameters are determined from fits to experimental data (Dunne et al., 2016), and $[n\pm]$ is the ion concentration produced from galactic cosmic rays (Sect. S2). A temperature dependence for the organic nucleation rates was introduced by multiplying by $\exp(-(T - 278)/10)$, as suggested in Dunne et al. (2016).

2.2.4 Updated particle growth scheme

The growth rate of nuclei is important for the survival probability up to larger sizes and eventually for a contribution to CCN (Pierce and Adams, 2009; McMurry et al., 2005). The effective production rate of 20 nm diameter particles (the smallest size simulated by the model) is calculated using the Kerminen and Kulmala (2002) formula:

$$j_{20\,\text{nm}} = j_{1.7\,\text{nm}}\exp\left[-\left(\frac{1}{1.7} - \frac{1}{20}\right)\frac{\gamma\text{CS}'}{\text{GR}}\right], \tag{9}$$

where CS$'$ is the reduced (simplified) condensation sink, γ is a proportionality factor, and GR is the growth rate. The reduced (simplified) condensation sink (CS$'$) is calculated as (Kerminen and Kulmala, 2002):

$$chemCS' = \frac{\text{CS}}{4\pi D_i}, \tag{10}$$

where CS is the condensation sink and D_i is the vapor diffusion coefficient. CS$'$ largely depends on CS and represents the surface area of preexisting aerosols.

In the Default simulation, sub-20 nm particle growth is solely caused by condensation of H_2SO_4 and is approximated by Kerminen and Kulmala (2002):

$$\text{GR} = \frac{3.0 \times 10^{-9}}{\rho}v_{H_2SO_4}M_{H_2SO_4}c_{H_2SO_4}, \tag{11}$$

where $v_{H_2SO_4}$ is the mean molecular speed of H_2SO_4, $M_{H_2SO_4}$ is the molecular weight of H_2SO_4, $c_{H_2SO_4}$ is the gas-phase concentration of H_2SO_4, and ρ is the density of the nuclei; 3.0×10^{-9} is an approximation of the product of many parameters (Kerminen and Kulmala, 2002).

Neglecting organic vapor condensation on sub-20 nm particles will lead to insufficient growth rates and potentially reduced survival of newly formed particles (Pierce and Adams, 2009). Therefore, the condensation of monoterpene-derived condensable organic compounds (COCs), including HOMs and ACC, to newly formed particles is added in our updated model. The enhanced growth rate of particles from 1 to 20 nm is then parameterized as follows:

$$\text{GR} = \frac{3.0 \times 10^{-9}}{\rho}(v_{H_2SO_4} \times M_{H_2SO_4} \times c_{H_2SO_4}$$
$$+ v_{\text{COC}} \times M_{\text{COC}} \times [c_{\text{COC}} - c^*_{\text{COC}}]), \tag{12}$$

where v_{COC} is the mean molecular speed of COCs (ACC and HOMs); M_{COC} is the molecular weight of COCs; c_{COC} is the gas-phase concentration of COCs; and c^*_{COC} is the saturated vapor concentration of COCs, which is parameterized in Sect. S3.

Simulations with the updated inorganic nucleation scheme (i.e., Eqs. 2–5) are named "Inorg", and simulations also including the new organic mechanisms (i.e., Eqs. 6–8 and 12) are named "Inorg_Org" (Table 2).

2.3 Method of evaluating NPF-related variables

In addition to evaluating aerosol concentrations, we also evaluate NPF event properties in terms of the nucleation rate, growth rate, and frequency of occurrence of NPF events. CAM6-Chem does not incorporate a nucleation mode, so we employ a threshold of $j_{20\,\text{nm}}$ (Eq. 9) to define the occurrence of NPF events (i.e., when $j_{20\,\text{nm}} >$ threshold). Then we could evaluate the NPF frequency (fraction of days) by defining an "NPF day" as a day during which $j_{20\,\text{nm}}$ is higher than a threshold value. Also, the method to evaluate these NPF properties during the NPF day is described in Sect. S4.

CAM6-Chem utilizes a four-mode version of the Modal Aerosol Module (MAM4) (Liu et al., 2016), including Aitken mode (with diameter 9 to 52 nm), accumulation mode (54 to 480 nm), coarse mode (400 to 40 000 nm), and primary mode (10 to 100 nm). The integral concentration from 0 to r_p is computed using the error function (erf):

$$N_{>r_p} = N_{\text{mode}}\left(\frac{1}{2} + \frac{1}{2}\text{erf}\left(\frac{x}{\sqrt{2}}\right)\right), \tag{13}$$

where x is defined as

$$x = \frac{\ln(r_p/r_m)}{\ln\sigma}, \tag{14}$$

where σ is the geometric standard deviation (the width) of the lognormal distribution and r_m is the median radius of the

mode. The integral concentration above r_p is therefore calculated as

$$N_{>r_p} = N_{mode} - N_{<r_p}. \tag{15}$$

The temporal frequency of the nucleation rate, growth rate, and condensation sink written out of the model is hourly, and the simulation periods are consistent with the observation period (with an additional month for spin-up). For aerosol number concentrations (including over oceans and land), the model outputs data on a monthly basis, and we compare these monthly averages with observations. When comparing the aerosol and CCN number concentrations with the field campaign in the Amazon basin, the output frequency from the model is hourly. Then, we slice the aircraft measurements of aerosol and the CCN number concentration vertical profiles according to the model output dimensions (four dimensions including time, height, latitude, and longitude). We average all measurement data within each slice and compare them with the corresponding model output data.

2.4 Sensitivity experiments

We performed two simulations to quantify the relative contributions of the nucleation rate (Only_NR) and growth rate (Only_GR) to aerosol concentrations in order to separate the contribution of the organic compounds to each of these processes. The Only_NR and Only_GR simulations employ the same settings as Inorg_Org (Table 2), but in Only_NR, the organic-involved particle growth is disabled (i.e., Eq. 11 is used instead), and in Only_GR, the organic-involved nucleation rates (i.e., Eqs. 6–8) are disabled.

We also conducted two sensitivity simulations to examine uncertainties in concentrations of HOMs (Table 2): sensitivity to the branching ratio from the first generation of monoterpene (MT) reactions with O_3/OH that can be auto-oxidized (Low_Br) and sensitivity to the rate of termination reaction involving NO (Slow_NO), sensitivity to the autoxidation temperature dependence (High_temp and Low_temp), sensitivity to the autoxidation rate (Fast_auto and Slow_auto), and sensitivity to the self- and cross-reaction rate (Slow_accr) (Table 2). In Inorg_Org, the branching ratios for the MT-derived peroxyl radicals (MT-RO$_2$), which can be further auto-oxidized are set at 80 % for MT + O_3 and 97 % for MT + OH reactions, corresponding to the high values reported in Xu et al. (2022). In the Low_Br simulation (Table 2), the branching ratio for MT-RO$_2$ is set as 25 % for MT + O_3 and 92 % and MT + OH. Both the high and low branching ratios fall within the range of previous studies (Lee et al., 2023; Pye et al., 2019; Weber et al., 2020; Xu et al., 2018; Jokinen et al., 2015; Roldin et al., 2019). In Slow_NO, the reaction rate of MT-HOM-RO$_2$ + NO (MT-HOM-RO$_2$, the second-generation product of autoxidation (Sect. S1), is set as one-fifth of that in Inorg_Org, given that the simulated NO concentration is 4-fold higher than the measured values in the boreal forest in Finland and in the southeast

USA (Figs. S3 and S2 in Liu et al., 2024). In High_temp and Low_temp, the temperature dependence of the autoxidation rate is set to lower and upper limits (i.e., representing the possible higher and lower bound of activation energy; Table S8) based on chamber experiments (Roldin et al., 2019; Weber et al., 2020). In Fast_auto and Slow_auto, the autoxidation reaction rates are multiplied by 10 and 0.1, respectively. In Slow_accr, the rate of self- and cross-reactions are set as the lower value (Table S9) based on chamber experiments (Weber et al., 2020; Berndt et al., 2018).

2.5 Observation data

Observational data used in this study are from ships, stations, and aircraft (see Table 3). Measurements from the Canadian Aerosol Baseline Measurement Program (CABM), the Reactive Halogens in the Marine Boundary Layer (RHaMBLe), and Aerosol–Cloud Coupling and Climate Interactions in the Arctic (ACCACIA) are compared with simulated N10 or N20 (number concentrations for particles with diameters larger than 10 or 20 nm), since these two variables are most sensitive to aerosol nucleation and initial growth. European Aerosol Cloud Climate and Air Quality Interactions projects (EUSAAR-EUCAARI) (Asmi et al., 2011; Kulmala et al., 2009) provide measured N30 and N50 (number concentrations for particles with diameters larger than 30 and 50 nm, respectively), and these larger particles are more important for the condensation sink (CS) of HOMs and other precursor vapors during NPF. All of the above-mentioned data were processed in the Global Aerosol Synthesis and Science Project (GASSP) (Reddington et al., 2017). Measured N20 and CCN concentrations at 0.5 % supersaturation from the aircraft campaign Aerosol, Cloud, Precipitation, and Radiation Interactions and Dynamics of Convective Cloud Systems (ACRIDICON–CHUVA) (Wendisch et al., 2016) are used to examine the effect of the inclusion of organic NPF on the profile of CCN concentrations in an organic-dominated tropical environment. We also use ground station measurements of nucleation rates, growth rates, CS, and NPF frequencies during specific time periods that correspond to the simulations. Full information of stations is listed in Tables S1 and S2 in the Supplement.

2.6 Evaluation of the updated NPF scheme

In this section, we evaluate the results derived from the updated model (Inorg_Org) and focus on the comparison between Inorg_Org and Inorg (definitions in Table 2). Specifically, we compare the nucleation rate, sub-20 nm particle growth rate, NPF event frequency, and condensation sink (CS) (Fig. 1) between simulations and measurements. Results from sensitivity tests (Low_Br and Slow_NO) are used to evaluate the effect of uncertainties in HOM chemistry on aerosol (Figs. 2 and 3) and CCN concentrations (Fig. 4).

Table 3. Field measurements used in this study.

| Campaign	Platform	Dates	Region	Variables
RHaMBLe (http://www.cas.manchester.ac.uk/resprojects/ rhamble/cruise/, last access: 3 October 2024)	Ship	17 May–9 Jun 2007	North Atlantic Ocean (16.32–46.14° N, 25.05–8.35° W)	N10
ACCACIA (https://catalogue.ceda.ac.uk/uuid/ ba055025cbaa430f988a2ca62320a774/, last access: 4 October 2024)	Ship	12 Jul–13 Aug 2013	Arctic between Norway and Svalbard (55.73–83.32° N, 20.70–34.84° E)	N10
CABM (https://ec.gc.ca/air-sc-r, last access: 4 October 2024)	Station	23 Oct 2012–1 Jan 2013	Ellesmere Island, Canada (82.49° N, 62.34° W) Egbert, Canada (44.23° N, 79.78° W)	N20
EUSAAR-EUCAARI (Asmi et al., 2011)	Station	1 Jan 2008–1 Jan 2010	Europe	N30, N50
ACRIDICON–CHUVA (Andreae et al., 2018)	Aircraft	September 2014	Amazon basin	N20 CCN (0.5 % ss)
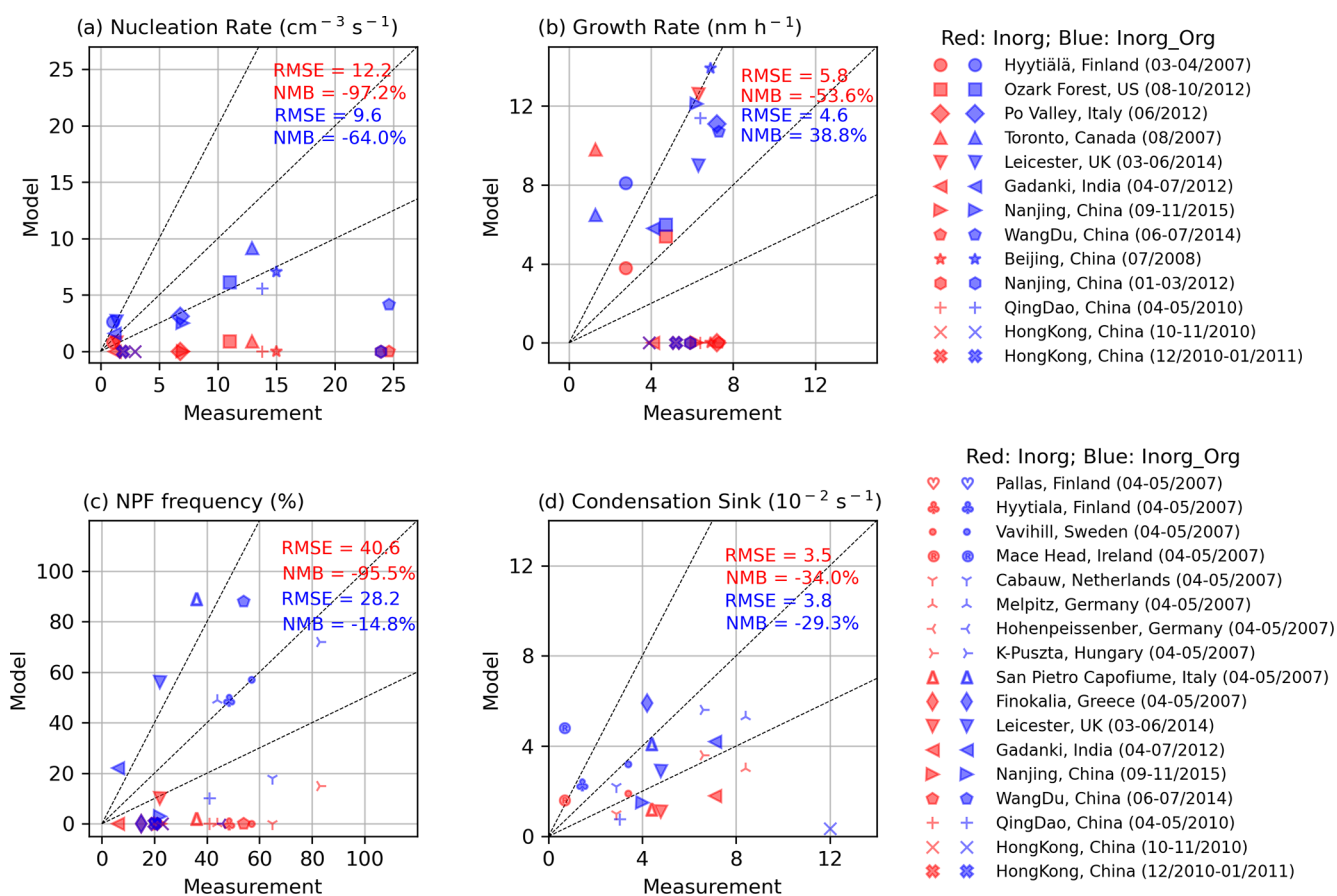
Figure 1. Comparison of simulated (choosing median value of measured smallest nucleation rates as threshold; see Sect. S4) and measured **(a)** nucleation rate, **(b)** growth rate, **(c)** NPF frequency, and **(d)** condensation sink in Inorg_Org (blue symbols) and Inorg (red symbols). Information regarding the measurement sites is summarized in Table S1. Root mean square error (RMSE) and normalized mean bias (NMB) values are shown. Panels **(a)** and **(b)** use the same dataset. Panels **(c)** and **(d)** use the same dataset.
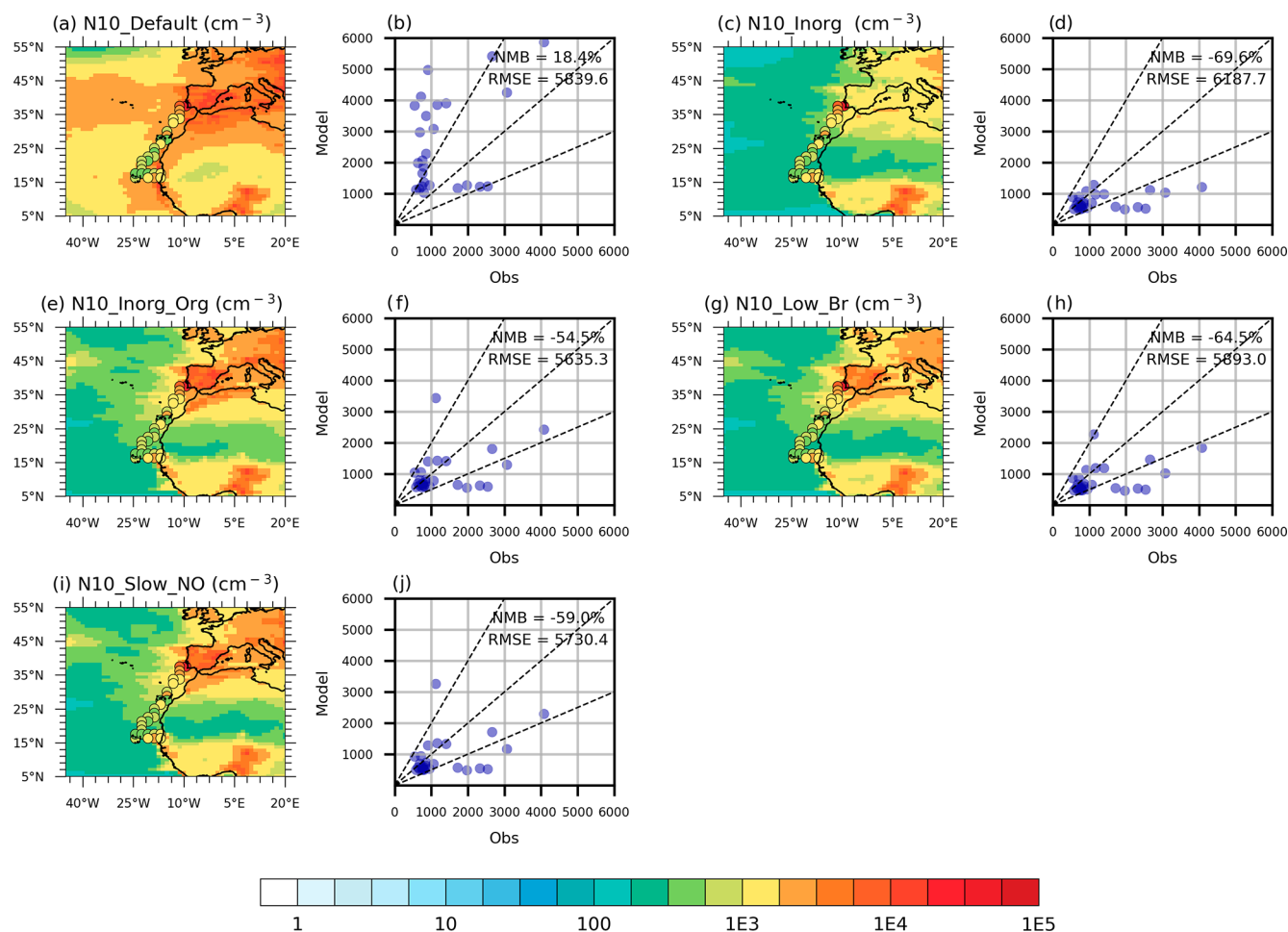
Figure 2. N10 concentration in the North Atlantic from **(a, b)** Default, **(c, d)** Inorg, **(e, f)** Inorg_Org, **(g, h)** Low_Br, and **(i, j)** Slow_NO (unit: cm^{-3}). N10 concentrations from RHaMBLe measurements are represented by filled circles. Model experiments are described in Table 2, and model data come from mean values of May 2007 outputs. Numbers in the upper right (Fig. 2b, d, f, h, and j) indicate normalized mean bias (NMB) and root mean square error (RMSE).

2.7　Evaluation of NPF-related variables

The properties of the nucleation events themselves (formation rates, growth rates, and event frequencies) provide the best test of NPF schemes, while state variables like particle concentration have many other sources of error in a model.

As shown in Fig. 1a, at most grounds stations, the nucleation rate in Inorg_Org agrees better with measurements than Inorg (normalized mean bias, NMB changes from -97% in Inorg to -64% in Inorg_Org). The improvement is particularly clear in non-urban areas where biogenic-organic nucleation plays a substantial role, such as Hyytiälä, Ozark Forest, Po Valley, and Leicester (NMB changes from -92% in Inorg to -34% in Inorg_Org, Fig. 1a). In these regions, the nucleation rate increases by at least a factor of 8 when the organic nucleation mechanisms are included (Inorg_Org compared to Inorg). In Toronto and Gadanki, the nucleation rate becomes detectable following the incorporation of organic

nucleation mechanisms, in good agreement with observations ($9.2\,cm^{-3}\,s^{-1}$ in Inorg_Org compared to $12.9\,cm^{-3}\,s^{-1}$ measurement of Toronto; $1.6\,cm^{-3}\,s^{-1}$ in Inorg_Org compared to $1.2\,cm^{-3}\,s^{-1}$ in measurement of Gadanki, Table S4). However, in multiple urban regions of China, the nucleation rate remains underestimated (NMB $> -50\%$). This is likely because the effects of anthropogenic-derived HOMs and amines are not accounted for in this study, and these effects will be strongest in urban regions. Hong Kong SAR serves as a stark example, where the nucleation rate shows minimal change when the biogenic-organic nucleation scheme is implemented, rising slightly from $0.3\,cm^{-3}\,s^{-1}$ (Inorg) to $0.31\,cm^{-3}\,s^{-1}$ (Inorg_Org). Several other Chinese megacities, including Beijing and Nanjing, show similar behavior.

Figure 1b shows that the growth rate in Inorg is underestimated (NMB $= -54\%$) but is overestimated at most sites in Inorg_Org (NMB $= 39\%$). The underestimation of the sub-20 nm growth rate in Inorg is due to an almost zero nucleation
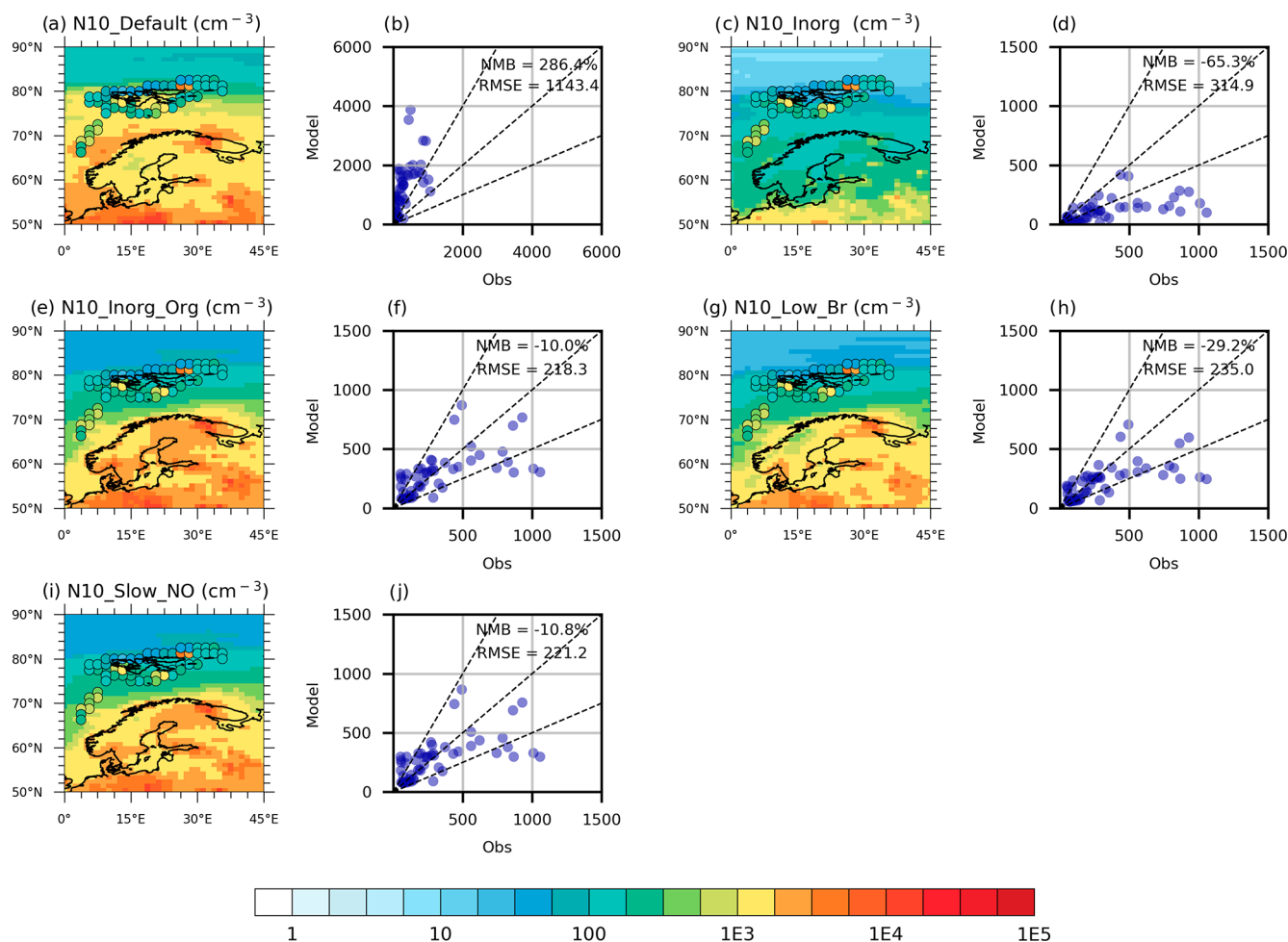
Figure 3. N10 concentration in the Arctic from **(a, b)** Default, **(c, d)** Inorg, **(e, f)** Inorg_Org, **(g, h)** Low_Br, and **(i, j)** Slow_NO (unit: cm^{-3}). N10 concentrations from ACCACIA measurements are represented by filled circles. Model experiments are described in Table 2, and model data come from mean values of July 2013 outputs. Numbers in the upper right (Fig. 3b, d, f, h, and j) indicate NMB and RMSE.

rate at around 1 nm. Consequently, the absence of a nucleation rate results in the absence of NPF events and thus a zero growth rate. In contrast, in Inorg_Org, the NPF frequency is simulated accurately compared to Inorg (Fig. 1c). One contributing factor to the overestimation of the growth rate in Inorg_Org is the overestimation of the H_2SO_4 concentration, a feature of CAM6, as evidenced by comparisons with previous model simulations (Table S6) and measurements (Table S7). This discrepancy is particularly noticeable in China, where H_2SO_4 dominates the growth rate (further discussed in Fig. 7, Sect. 3). This is also supported by overestimated growth rates in Beijing, Qingdao, and Hong Kong SAR in Inorg, which only considers the H_2SO_4 contribution to sub-20 nm growth. This suggests excessive H_2SO_4 is a feature of the default model. The growth rate of new particles in Hong Kong SAR is zero (Fig. 1b) since there are almost no newly formed particles (nucleation rate $\sim 0\,cm^{-3}\,s^{-1}$, Fig. 1a).

NPF events are far more frequent in Inorg_Org than in Inorg (NMB in NPF frequency changes from -96% to

-15%) (Fig. 1c). Simulated NPF frequencies in Inorg_Org agree better with measurements in Europe (Hyytiälä, Vavihill, Cabauw, Melpitz, and K-Puszta) – see Table S5. Inorg_Org tends to overestimate NPF frequencies (by a factor of 2) in some rural and forested areas such as the San Pietro Capofiume, Leicester, and Wangdu and significantly underestimates frequencies in Chinese urban areas like Nanjing and Hong Kong SAR (more than 3 times; Fig. 1a). These discrepancies are consistent with the nucleation rates discussed earlier (Table S4). In some locations (Melpitz, San Pietro Capofiume, Leicester and Gadanki) the overestimation of NPF frequency in Inorg_Org is consistent with an underestimation of CS, and, vice versa, the underestimation of NPF frequency in Finokalia is consistent with an overestimation of CS (Fig. 1c and d).
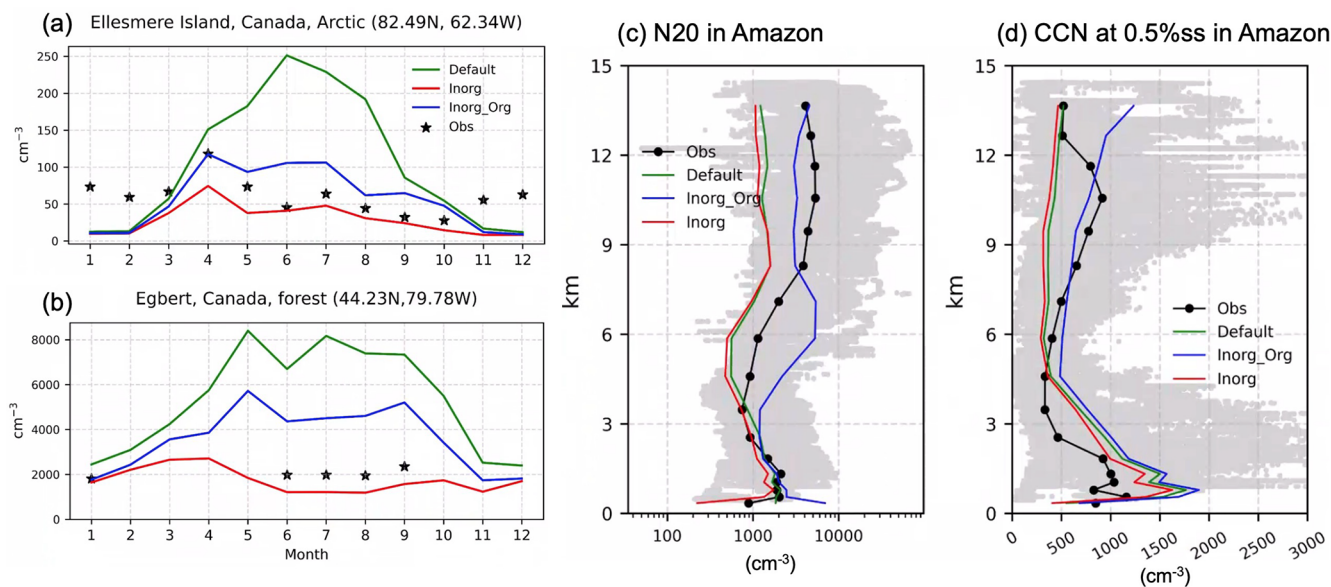
Figure 4. Seasonal variation in 2013 at two Canadian sites: **(a)** Ellesmere Island and **(b)** Egbert. Vertical profiles of **(c)** N20 and **(d)** CCN at a supersaturation of 0.5 % in the Amazon basin, measured at standard temperature and pressure (STP) (unit: cm^{-3}), in September 2014.

2.8 Evaluation of aerosol and CCN number concentrations

To better understand the influence of implementing the new nucleation schemes, model-simulated particle number concentrations are evaluated against shipborne measurements over the ocean, and CCN concentrations are evaluated using measurements from Amazonia. We also discuss the influence of uncertainties in HOM chemistry. Unlike Spracklen et al. (2010), the lack of a nucleation mode in CAM means that we cannot use extensive measurements from condensation particle counters.

The values of number concentrations for particles with diameters larger than 10 nm (N10) in Inorg_Org agree better with measurements over the ocean (Figs. 2 and 3), but number concentrations for particles with diameters larger than 20 nm (N20) are overestimated in continental regions at the surface level (Fig. 4). From Figs. 2 and 3, N10 concentrations in Inorg_Org are the closest to measurements in both the North Atlantic and the Arctic when considering both normalized mean bias (NMB) and root mean square error (RMSE). Inorg_Org (Figs. 2e, f and 3e, f) alleviates both overestimation of N10 in Default resulting from their high sensitivity to H$_2$SO$_4$ concentrations (see Figs. 2a, b and 3a, b) and underestimation at some sites in Inorg caused by the lack of organics participating in NPF (Figs. 2c, and 3c, d). The influence of HOM chemistry to N10 will be discussed in Sect. 5. In boreal Canada (Fig. 4), N20 concentrations are overestimated in Inorg_Org during the summer when NPF is particularly active. The overestimation is more significant at Egbert, located just 80 km north of Toronto, where Inorg shows better agreements with measurements. This discrepancy is likely due to

an about 30 % overestimation of growth rates (in Toronto, Table S4) and the underestimation of N50 during northern hemispheric summer (as relevant to CS) at many stations in Inorg_Org (N50 in Fig. S9). The underestimation of N50 also explains the overestimation of N20 observed at the surface level in Amazonia in September 2014 (Fig. 4c), where insufficient large aerosols (N50, Fig. S9) result in a low CS, which in turn leads to an excessive number of aerosols merging into the Aitken mode (N30, Fig. S8).

After incorporating organic-related processes, CCN at high altitudes of Amazonia perform better compared with measurements. While all simulations considerably overestimate CCN concentrations at 0.5 % supersaturation (0.5 % ss) at surface level, CCN in the upper troposphere (5–12 km) in Inorg_Org (blue line, Fig. 4d) are the closest to measurements compared with both Default and Inorg. The more than 100 % increase in CCN numbers at 8–12 km is mainly attributed to effective vertical transport of accretion products (ACC), which have a longer atmospheric lifetime compared to HOMs (Xu et al., 2022) and then participate in $J_{Org,n}$ and $J_{Org,i}$ (Fig. 6c and e), thereby increasing N20 and CCN concentrations at high levels. N20 shows the highest value at about 6 km altitude since nucleating species are abundant there, and the condensation sink is relatively low (see CCN profile in Fig. 4d) compared to higher altitudes. Since we did not consider the suppression of C15 generated from isoprene- and monoterpene-derived RO$_2$ (MT-RO$_2$) radicals cross-reactions on nucleation rates (Heinritzi et al., 2020), the ion-induced pure organic nucleation rate is overestimated in Amazon, and hence, cloud condensation nuclei (CCN) at surface level are overestimated in Inorg_Org.
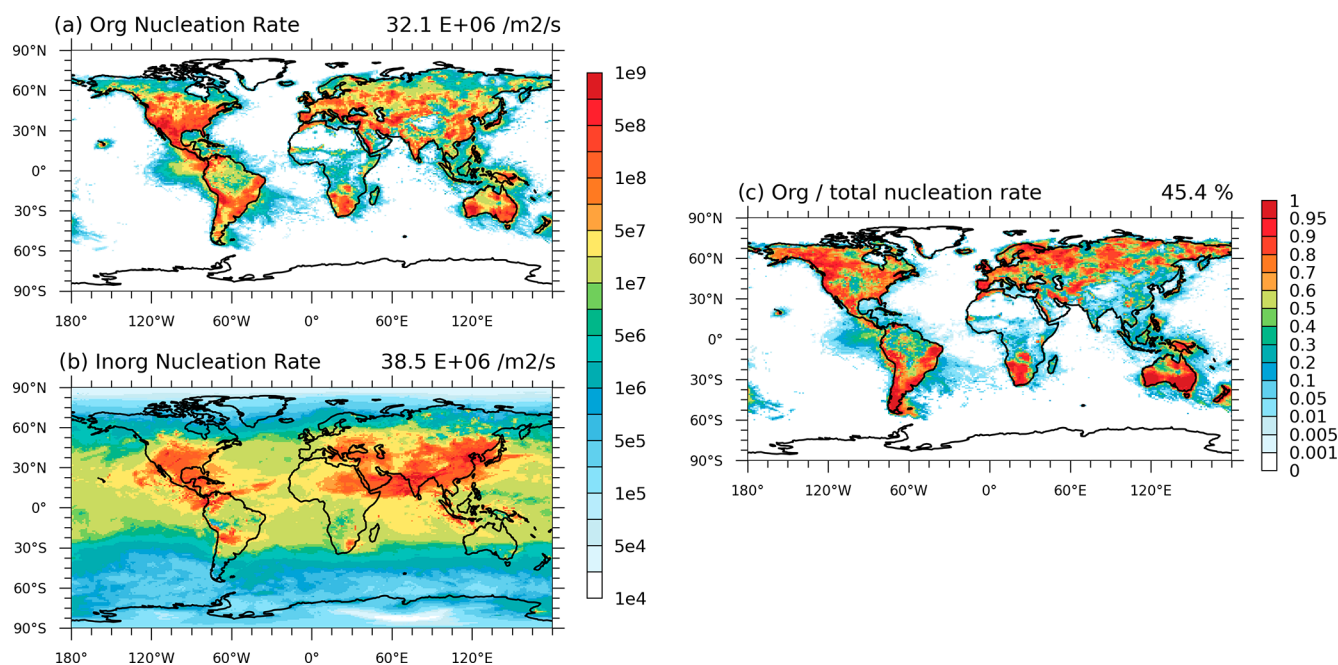
Figure 5. Spatial distribution of the 2013 annual mean nucleation rate ($j_{1\,nm}$, vertically integrated below 15 km) attributed to **(a)** organics and **(b)** H_2SO_4 (unit: $m^{-2}\,s^{-1}$). Panel **(c)** shows the proportion of organic nucleation proportion. Global mean values are shown in the top right of each figure.

3   Quantifying the effect of organics' NPF on global aerosol

In this section, we use simulation results to quantify how HOMs affect the nucleation rate (Figs. 5 and 6), growth rate (Fig. 7), particle number (Fig. 8), and CCN number (Fig. 10) on a global scale. Additionally, results from sensitivity tests (Table 2) are also analyzed to reveal the influence of uncertainty from chemical mechanisms of HOMs and the relative importance of organic nucleation and initial growth process to particle number (Fig. 9).

Globally, the vertically integrated (below 15 km) annual mean organic nucleation rate ($J_{Org,n} + J_{Org,i} + J_{SA-Org}$) in Inorg_Org is $32 \times 10^6\,cm^{-2}\,s^{-1}$ (Fig. 5a), closely matching the inorganic nucleation rate of $39 \times 10^6\,cm^{-2}\,s^{-1}$ (Table 4). J_{SA-Org} contributes most to the total nucleation rate (45 %), with an average value of $31.8 \times 10^6\,cm^{-2}\,s^{-1}$ (Table 4), and its spatial distribution (Fig. 6a) is influenced by both H_2SO_4 and HOM concentrations. In regions abundant in HOMs (like boreal forests, North America and Australia in Fig. S5), the rate surges to $10^8\,cm^{-2}\,s^{-1}$ (Fig. 5a) and the organic contribution exceeds 80 % (Fig. 5c). High concentrations of ACC are simulated in Amazonia (Fig. S6), where ACC products are transported to high altitudes through strong convection (Sect. 2.6), thereby resulting in high rates of $J_{Org,i}$ (over 40 %, Fig. 6f). H_2SO_4–NH_3 neutral nucleation comprises the largest proportion of the inorganic nucleation rate (> 80 % of inorganic and 40.5 % of total nucleation rate, Table 4), particularly in China and India due to high anthropogenic SO_2

Table 4. The 2013 annual average vertically integrated organic nucleation rate ($j_{1\,nm}$) within the troposphere and its contributions to total nucleation rates in Inorg_Org.

Pathways	Nucleation rate (unit: $10^6\,m^{-2}\,s^{-1}$)	Proportion (%)
J_{SA}	3.09	4.38
$J_{SA,i}$	2.62	3.71
J_{SA-NH_3}	3.09	40.48
$J_{SA-NH_3,i}$	4.22	5.99
$J_{Org,n}$	0.40	0.01
$J_{Org,i}$	0.30	0.37
J_{SA-Org}	31.80	45.06

emissions. This is also consistent with the spatial distribution of H_2SO_4 (Fig. S4). The contribution of H_2SO_4–NH_3 neutral nucleation makes up more than 50 % of the nucleation rate over coastal regions where HOMs and accretion products (ACC) are less abundant (Figs. S5 and S6), and the large proportion in Africa is due to high NH_3 column concentration (Luo et al., 2022).

Globally, the vertically averaged (below 15 km) annual mean organic growth rate is $0.0048\,nm\,h^{-1}$ (summation of ACC and HOM contribution). The organic growth rate contributes to 25 % of the total growth rate for sub-20 nm particles. In regions such as Canada, the boreal forests, Amazonia, and Australia, where biogenic volatile organic compound (BVOC) emissions dominate, organic growth ac-
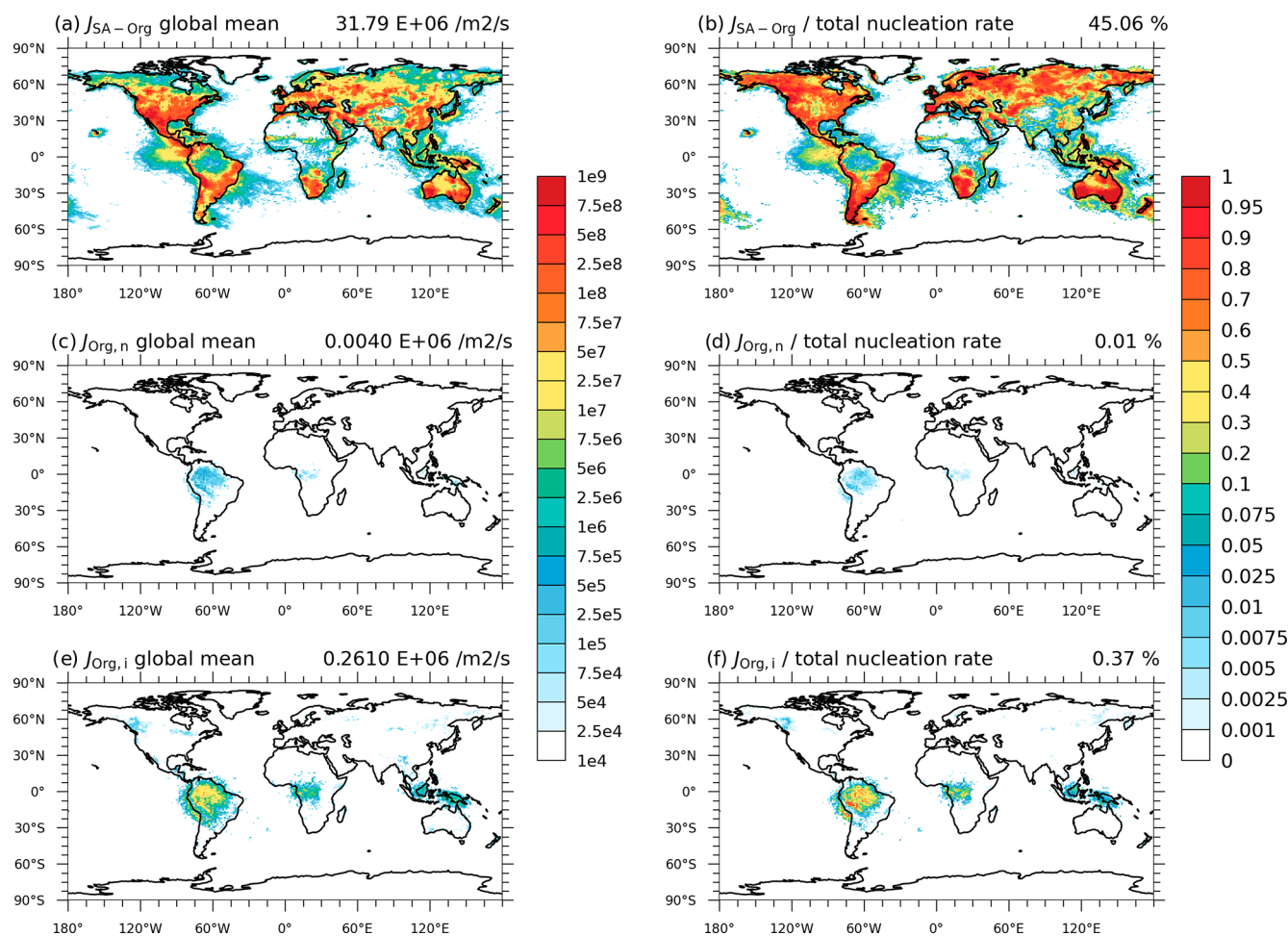
Figure 6. The 2013 annual average vertically integrated organic nucleation rate ($j_{1\,nm}$) within the troposphere (**a, c, e**) (unit: m^{-2} s^{-1}) and their respective contributions (**b, d, f**) for J_{SA-Org} (**a, b**), $J_{Org,n}$ (**c, d**), and $J_{Org,i}$ (**e, f**) in Inorg_Org. Global mean values are shown in the top right of each figure.

counts for over 60 % of the total rate (Fig. 7c), consistent with the spatial distribution of HOMs and ACC (Figs. S5 and S6). Conversely, in China and India, H$_2$SO$_4$ exerts a predominant influence ($> 90\,\%$) on the initial growth of new particles, with a rate of approximately 0.1 nm h^{-1}.

The global mean aerosol number burden increases by 39 % (Fig. 8) in Inorg_Org compared to Inorg. The enhancement reaches a maximum of 60 % in Amazonia due to high $J_{Org,i}$ (Fig. 6f) driven by high ACC concentrations (Fig. S6). Results from the Low_Br and Slow_NO simulations reveal that the uncertainties in HOM chemistry have a negligible effect on the total aerosol number concentrations. Relative to Inorg_Org, Low_Br leads to a 12 % reduction in number concentrations (Fig. 9f), although the branching ratio of MT-RO$_2$ shifts significantly (from 80 % to 25 % for the MT + O$_3$ reaction and from 97 % to 92 % for the MT + OH reaction). The impact of slowing down the reaction rate of MT-HOM-RO$_2$ + NO (Slow_NO) is negligible globally ($< 1\,\%$, Fig. 9h).

To evaluate the relative importance of organic contributions to nucleation and growth, we compare the Only_NR (no organic contribution to sub-20 nm particle growth rate) and Only_GR (no organic contribution to 1 nm particle nucleation rate) simulations. The global mean relative difference of aerosol number concentration between Only_GR (Fig. 9d) and Inorg_Org is 28 % in a 1 month simulation. Switching off growth alone (Only_NR) results in a 34 % decrease in aerosol number relative to Inorg_Org (Fig. 9b). This illustrates that organic initial growth of new particles (sub-20 nm) is slightly more important than organic nucleation for the production of particles larger than 20 nm diameter.

The global annual average CCN burden at 0.5 % supersaturation increases by 33 % after adding organic NPF (Fig. 10). The spatial pattern of changes in CCN concentrations compared to Inorg is consistent with changes in aerosol number concentrations (Fig. 8), with increases predominantly occurring in regions abundant in HOMs and ACC (Figs. S5 and S6). Amazonia is the region most sen-
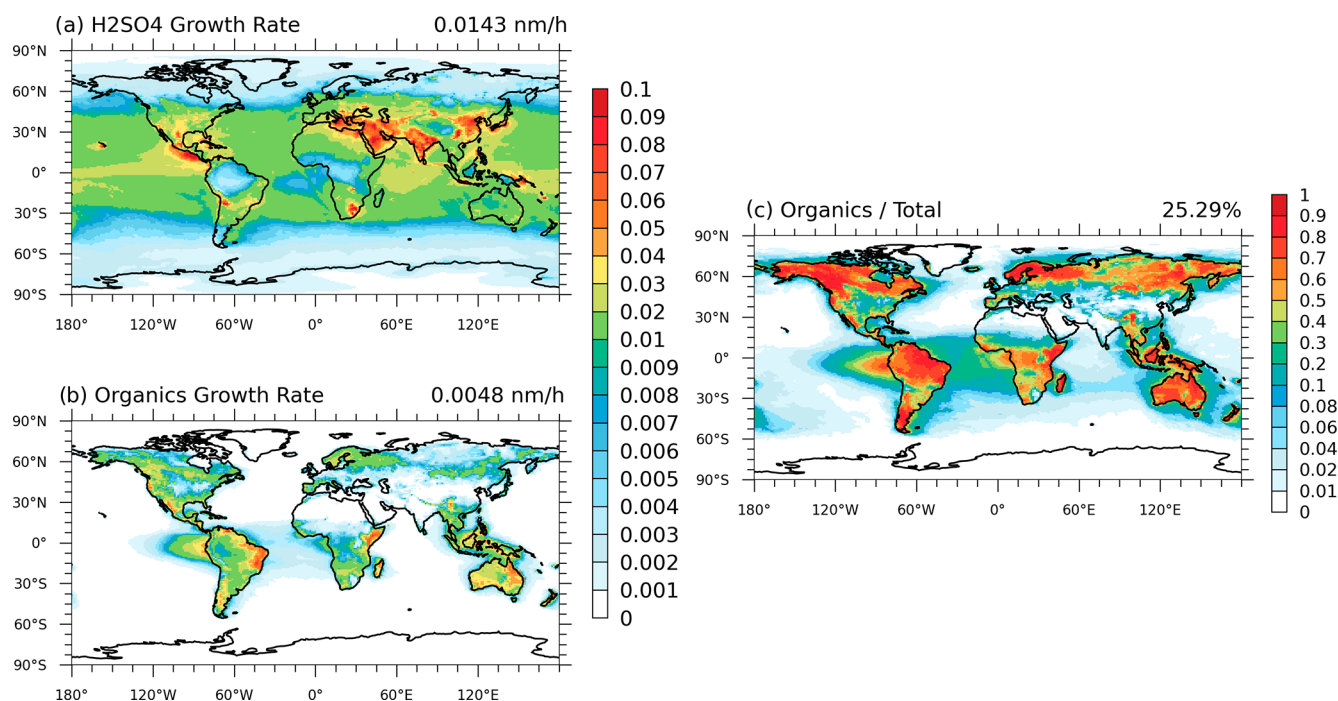
Figure 7. Spatial distribution of the 2013 annual mean vertically averaged growth rate attributed to **(a)** H_2SO_4 and **(b)** organics, along with the percentage of organics contributions **(c)**. Global mean values are shown in the top right of each figure.

Figure 8. Spatial distribution of annual mean total vertically integrated particle number concentrations from **(a)** Inorg and **(c)** Inorg_Org (unit: cm^{-2}). Also, **(b)** change and **(d)** relative change are shown. Global mean values are shown in the top right of each figure.

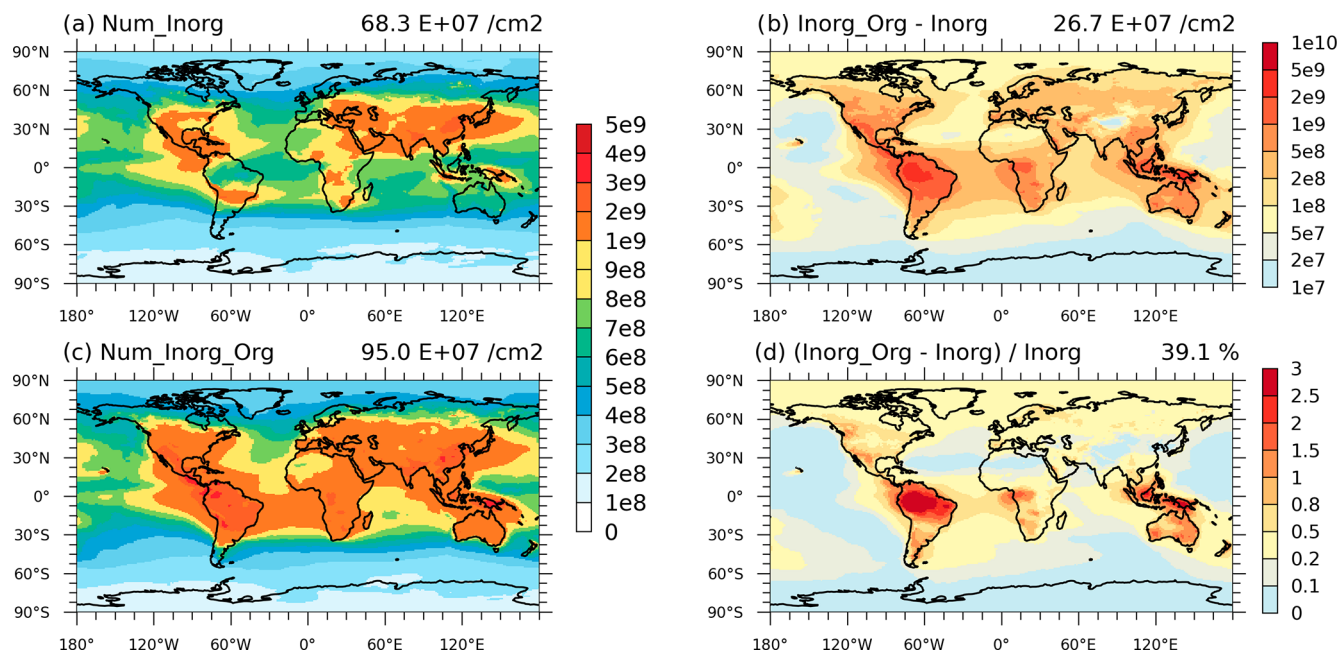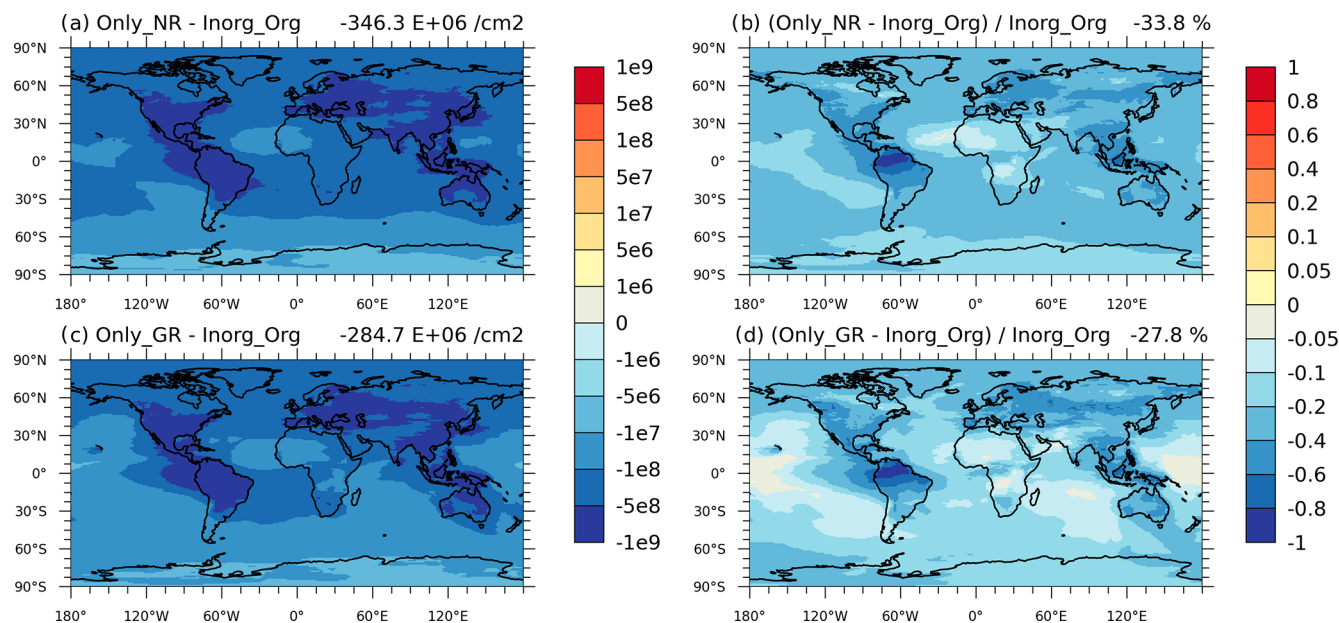**Figure 9.** Absolute differences (units: cm^{-2}) and relative differences (units: unitless) of in total vertically integrated aerosol numbers in July 2013 between Inorg_Org and other sensitivity tests. Global mean values are shown in the top right of each figure. Model experiments are described in Table 2.
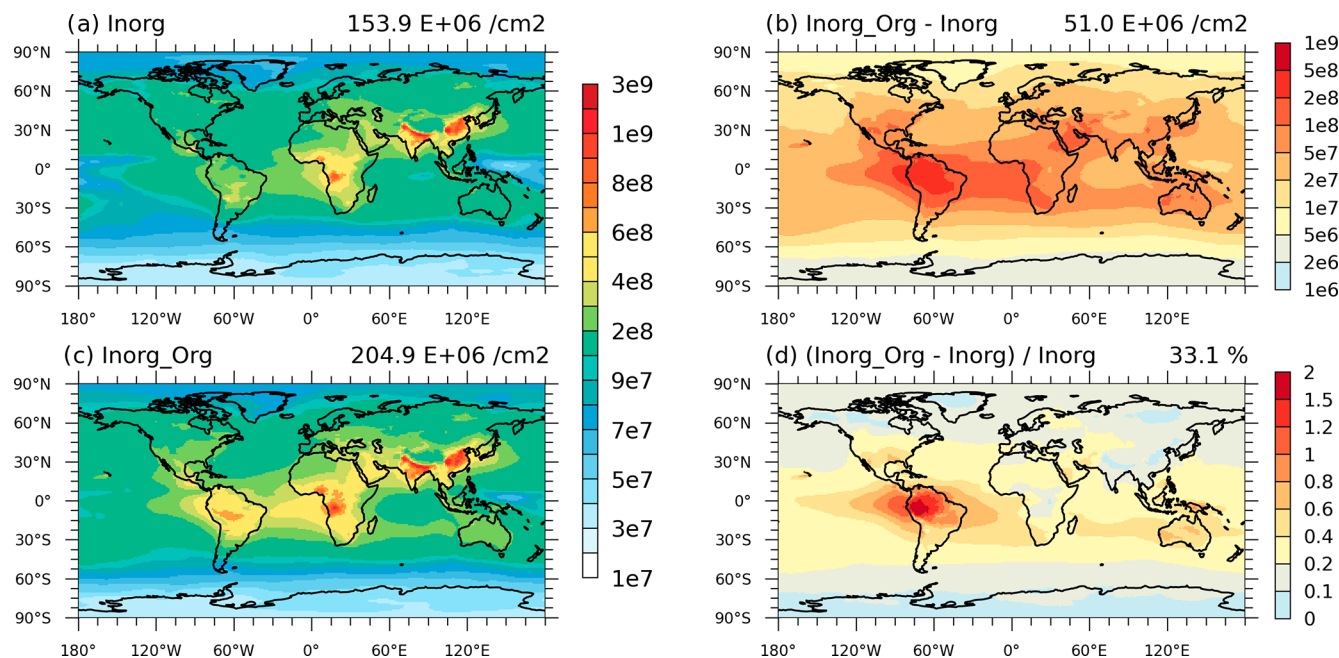
Figure 10. Spatial distribution of annual mean total vertically integrated CCN concentrations at 0.5 % supersaturation for **(a)** Inorg and **(c)** Inorg_Org (unit: cm^{-2}). Also, **(b)** change and **(d)** relative change are shown. Global mean values are shown in the top right of each figure.

sitive to organic-related processes due to high ACC concentrations (Fig. S6), where the total burden increases by more than 100 % (Fig. 10d).

4 Uncertainties from HOM chemistry

This section aims to test the effects of using different autoxidation and self- and cross reaction rates as well as branching ratios during HOM and ACC formation on the 1 nm nucle-

Table 5. Relative differences (units: unitless) of vertically integrated HOM concentrations (HOMs), accretion products concentrations (ACC), nucleation (NR), growth rate (GR), aerosol number (Aerosol), and CCN number (CCN) in July 2013 between Inorg_Org and other sensitivity tests. Values in the table are global mean values. Model experiments are described in Table 2.

	HOMs	ACC	NR	GR	Aerosol	CCN
Slow_NO	−6 %	5 %	−2 %	∼0	∼0	∼0
Low_br	−51 %	−12 %	−17 %	−5 %	−12 %	−5 %
High_temp	−42 %	−6 %	−7 %	−4 %	−12 %	−4 %
Low_temp	9 %	∼0	−4 %	∼0	3 %	∼0
Fast_auto	75 %	8 %	6 %	3 %	18 %	4 %
Slow_auto	−57 %	−5 %	−17 %	−5 %	−15 %	−6 %
Slow_accr	66 %	−71 %	−4 %	∼0	−2 %	−1 %

Table 6. Fractions of NPF from organic and inorganic pathways are derived from Inorg_Org (annual average in 2013 below 5.8 km altitude). Results from Gordon et al. (2017) and Zhu and Penner (2019) are in present-day experiments.

Pathways	Below 5.8 km vertical integration		
	Gordon et al. (2017)	Zhu and Penner (2019)	This study
J_{SA}	∼0	58.40 %	0.03 %
$J_{SA,i}$	7.50 %	w/o[a]	1.96 %
J_{SA-NH_3}	17.00 %	w/o	6.18 %
$J_{SA-NH_3,i}$	24.00 %	w/o	8.28 %
$J_{Org,n}$	∼0	0.60 %	∼0
$J_{Org,i}$	4.10 %	23.20 %	0.11 %
$J_{SA-Org,i}$ [b]	14.00 %	w/o	w/o
J_{SA-Org}	33.00 %	17.80 %	83.44 %

[a] w/o represents that there is no consideration of that nucleation scheme in publications. [b] $J_{SA-Org,i}$ represents ion-induced heteromolecular nucleation of sulfuric acid and organics (HET).

ation rate, sub-20 nm growth rate, total aerosol number concentration, and CCN number concentration.

The change of the autoxidation rate (Fast_auto and Slow_auto) affects both the nucleation and growth rates, particularly within HOMs source regions. A higher autoxidation rate leads to higher intermediate radical concentrations and thus more HOMs. Multiplying the autoxidation rate by 10 (Fast_auto) leads to a 6 % increase in the nucleation rate and a 3 % increase in the sub-20 nm growth rate on a global average (Fig. S11). The largest increases occur in regions such as the Amazon, Australia, and boreal forests (> 10 %), where HOMs are most abundant. In these regions, the aerosol number concentration increased by more than 30 % compared to the baseline Inorg_Org. Conversely, in Slow_auto, the nucleation and growth rates decline by 17 % and 5 %, respectively, resulting in a 15 % reduction in aerosol number and a 6 % reduction in CCN number globally. In the Amazon and boreal forests, these reductions exceed 20 % (Table 5).

Adjusting the autoxidation temperature dependence to upper and lower limits (High_temp and Low_temp) causes changes in HOM concentrations (Fig. S10). However, its impact on nucleation (−7 % and −4 % in High_temp and Low_temp), growth rate (−4 % and ∼0 % in High_temp and Low_temp), aerosol (−12 % and 3 % in High_temp and Low_temp), and CCN (−4 % and ∼0 % in High_temp and Low_temp) number concentrations is small (Fig. S11 and S12). This is because most of these changes occur over ocean, where H_2SO_4 has low concentrations. Consequently, the rate of heteromolecular nucleation of sulfuric acid and organics (HET), which is the greatest contributor to the organic-involving nucleation rate, does not show significant change in both experiments.

A lower dimerization reaction rate leads to decreased concentrations of accretion products (ACC), with a 71 % decrease in Slow_accr. Lower consumption of MT-derived peroxyl radicals (MT-RO_2) during self- and cross-reaction means more of them can participate in autoxidation. This explains the higher HOM concentration over source regions in Slow_accr compared to Inorg_Org (Fig. S10). However, the

impact of slowing down the dimerization rate on aerosol and CCN number concentrations is negligible, remaining within 1 % on a global average. In the Slow_accr experiment, the nucleation rate in the Amazon, where the concentration of ACC is highest, decreases by more than 50 %, subsequently leading to a reduction of more than 20 % in aerosol and CCN numbers (Table 5). This implies that both aerosol and CCN number concentrations in the Amazon basin are sensitive to the ACC concentration.

The change in HOMs and ACC concentrations in Slow_NO is almost negligible (−6 % and 5 %); hence its impact on aerosol and CCN number can be ignored (∼0 %). When the rate of NO termination is reduced, less MT-HOM-RO_2 is consumed when generating HOMs, and thus more MT-HOM-RO_2 participates in self- and cross-reactions. This explains the higher concentration of ACC and lower concentration of HOMs in Slow_NO compared to Inorg_Org. In contrast, in Low_Br, there is a significant decrease in HOM concentration (−51 %) (Fig. S10) since the mass yield of MT-bRO_2 decreases, which subsequently leads to a 17 % reduction in the nucleation rate (Fig. S11). Combining with approximately a 5 % reduction in the growth rate of sub-20 nm particles, the concentrations of aerosol and CCN decrease by −12 % and −5 %, respectively (Table 5). In regions most sensitive to biogenic HOM chemistry, such as the Amazon, Australia, and boreal forests, the reduction in particle concentrations exceeds 20 %.

5 Comparison with previous studies

Our results show that vertically integrated organic nucleation contributes 84 % of the total nucleation rate within the lower 5.8 km of the atmosphere, which is much higher than that in previous studies (51 % in Gordon et al. (2017) and 42 % in Zhu and Penner (2019); Table 6). The HOM concentrations in our simulations are about 10 times greater than in Gordon et al. (2017), as depicted in Figs. S7 and. S2 in Gordon

Table 7. Annually averaged NPF from three organic pathways: vertically integrated results across the whole atmosphere.

Pathways	Zhu and Penner (2019)[a]	This study[b]
J_{SA-Org}	34.4	33.0
$J_{Org,n}$	1.0	4.5×10^{-03}
$J_{Org,i}$	52.9	0.3
Total	88.2	33.2

[a,b] Results are compared between the present-day atmosphere (Zhu and Penner, 2019) and the 2013 annual mean in this study.

et al. (2016). Here we used a chemical mechanism of HOMs derived from chamber experiments (including both autoxidation and self- and cross-reactions of isoprene-/monoterpene-derived radicals), while Gordon et al. (2016) estimated HOM concentrations using an empirical fixed yield from monoterpene + O_3/OH. Higher HOM concentrations in our simulation are much closer to measurements in Finland and the southeast USA (Figs. S4 and S5 in Liu et al., 2024) and lead to higher J_{SA-Org}.

Updates to the inorganic nucleation scheme based on CLOUD chamber experiment data (Dunne et al., 2016) are the main reason we have higher contributions of vertically integrated organic nucleation than Zhu and Penner (2019). The updated scheme decreases the inorganic nucleation rate by reducing its sensitivity to H_2SO_4 concentration. Thus, we simulate a higher organic nucleation proportion despite much lower $J_{Org,i}$ and $J_{Org,n}$ (Table 7). The lower values of $J_{Org,i}$ and $J_{Org,n}$ are caused by our use of a more stringent definition of organic participation (only ACC products due to their extremely low or ultra-low volatility) in neutral and ion-induced pure organic nucleation (NON and ION; Eqs. 7 and 8).

6   Summary and discussion

This study updates the inorganic nucleation scheme in CAM6-Chem according to chamber experimental measurements and adds an organic nucleation and initial growth scheme based on a state-of-the-art chemical mechanism for biogenic highly oxygenated molecules (HOMs) including autoxidation and self- and cross-reactions of isoprene-/monoterpene-derived radicals. The organic nucleation scheme includes heteromolecular nucleation of sulfuric acid and organics (HET), neutral pure organic nucleation (NON), and ion-induced pure organic nucleation (ION). Organic condensation on sub-20 nm particles is also taken into account. The model was evaluated against new particle formation (NPF) events (occurrence frequency and nucleation and growth rates) as well as aerosol and cloud condensation nuclei (CCN) number concentrations. Finally, we quantified the contribution of organics to nucleation rate, growth rate, aerosol, and CCN number at 0.5 % supersaturation globally.

Compared to the model with updated inorganic nucleation mechanisms (Inorg), the revised model with HOM chemistry (Inorg_Org) agrees better with measurements of the nucleation rate and sub-20 nm particle growth rates at numerous sites globally (the normalized mean bias (NMB) of nucleation rate changes from −97 % to −64 %, and the NMB of growth rate changes from −96 % to −15 %; Fig. 1). Inorg_Org also simulates NPF event frequency, with better agreement with measurements at 17 sites compared to Inorg (NMB changes from −96 % to −15 %, Fig. 1), thereby accurately reproducing N10 (number concentrations for particles with diameters larger than 10 nm) ship-borne measurements over the Arctic and North Atlantic (Figs. 2 and 3). Both N20 (number concentrations for particles with diameters larger than 20 nm) and CCN concentration increase more than 100 % between 8–12 km altitude (Fig. 4) over Amazonia after incorporating organic-related process and show better performance compared to aircraft measurements due to organic nucleating species (accretion productions) convection lifting to high level and then amplifying $J_{Org,i}$ (ION rate).

On a global scale, organics contribute 45 % to the annual average vertically integrated nucleation rate and 25 % to the vertically averaged initial growth rate from Inorg_Org (global mean). Compared to Inorg, Inorg_Org increases the annual average vertically integrated aerosol number concentration by 39 %. The simulation shows that the organic-related growth process exerts a more substantial influence on aerosol number than nucleation. These newly formed particles result in a 33 % increase in annual average vertically integrated CCN concentrations at 0.5 % supersaturation compared to Inorg. Both aerosol and CCN concentrations display the most significant increase in Amazonia, exceeding 60 % and 100 %, respectively, attributable to its low aerosol concentration in Inorg in the background rainforest. More CCN produced through natural processes implies higher background aerosol abundance and thus weaker (less negative) historical aerosol forcing (Carslaw et al., 2013).

We also test the sensitivity of aerosol number concentrations to uncertainties from HOM chemistry. Results show that including organic NPF processes in our model is more important than tuning these aspects of the parameterizations during HOM formation. Compared to the baseline Inorg_Org model, decreasing the branching ratio of the first-generation product from monoterpene + O_3/OH, which could further undergo autoxidation (Low_Br), leads to only a 12 % reduction in global average vertically integrated aerosol number concentrations. Slowing down NO-involved chemical reactions due to NO concentration overestimation at two stations (Slow_NO) has very little effect on the global average aerosol number concentration (within ∼ 1 %) (Fig. 10). When altering the temperature dependence of autoxidation rate to a higher or lower value (High_temp and Low_temp), HOM concentrations change a lot (−42 % and 9 %, respectively), but aerosol number concentrations only change a small amount (−12 % and 3 %). Factor-of-10 changes in au-

toxidation rate (multiplying the autoxidation rate by 10 in Fast_auto and 0.1 in Slow_auto) result in relatively significant changes in the simulated aerosol number concentration (18 % and −15 % in global mean). When adjusting the dimerization rate coefficient of ACC formation to a lower value (Slow_accr), the aerosol number change is negligible (within 2 % on global average). Except for Amazon, the aerosol number concentrations are highly sensitive to ACC concentration and decrease by more than 20 %.

The contribution of organic-involved nucleation to the vertically integrated rate within the lower 5.8 km in our work (∼ 83 %) is significantly higher than previous studies. Compared to Gordon et al. (2017) (∼ 51 %), we use a more advanced HOM chemistry that simulates higher HOM concentrations in closer to measurements, thereby presenting a higher J_{SA-Org} (HET rate) and organics contribution. Compared to Zhu and Penner (2019) (∼ 42 %), we update the inorganic nucleation scheme based on CLOUD chamber experiments. Therefore, the inorganic nucleation rate and its proportion are reduced in our simulations, and this provides a more reasonable baseline for the quantifying organic contribution. The greater contribution of biogenic-organic nucleation to NPF implies that global aerosol may be more sensitive to changes in biogenic emissions. This finding should be tested with different Representative Concentration Pathways (RCPs) in the future, when human-induced global warming causes higher temperature and biogenic HOM emissions, while emission reduction policies reduce anthropogenic emissions.

The chemical mechanisms of biogenic HOMs used in this study are state-of-the-art, but the largest uncertainties in this work still come from the chemical mechanisms of HOMs and thus HOM concentration. Although we only consider two-step autoxidation reactions which are not the most advanced (Heinritzi et al., 2020; Simon et al., 2020), this impact on organic nucleation rate is almost negligible. Specifically, the number of autoxidation steps has almost no effect on the rate of heteromolecular nucleation of sulfuric acid and organics (HET), which is the most significant contributor to organic nucleation rate (Fig. 6 in the main text). This is mainly because the number of autoxidation steps affects neither the yield nor the concentration of C10-HOMs, only their molecular formulas and volatility. In our simulation, the lower volatility of C10-HOMs does not affect their participation in HET (i.e., LVOCs, ELVOCs and ULVOCs can all contribute to HET), so the rate of HET is not influenced by the number of autoxidation steps. Previous studies (Kurtén et al., 2016; Tröstl et al., 2016) have already indicated that C10 class molecules alone do not have low enough vapor pressure to initiate the nucleation, without the presence of other species such as sulfuric acid or bases. This is further supported by the fact that C20 class molecules are mainly responsible for pure biogenic nucleation (Heinritzi et al., 2020; Frege et al., 2018). This means that C10-HOMs might become less volatile when undergoing one additional autoxidation step,

transitioning from LVOCs ($3 \times 10^{-5} < C^*(T) < 0.3\,\mu\text{g m}^{-3}$, where $C^*(T)$ is the effective saturation concentration) to ELVOCs ($3 \times 10^{-9} < C^*(T) < 3 \times 10^{-5}\,\mu\text{g m}^{-3}$), but this is unlikely to affect the pure organic nucleation rate.

There might be some overestimations with C15 and C20 involved in new particle formation if we assume that all the accretion products are ELVOCs or ULVOCs. In the updated model, $C_{15}H_{18}O_9$ (C15, extremely low volatility) and $C_{20}H_{32}O_8$ (C20, ultra-low volatility) are just simplified representatives of all C15 and C20 dimers. While more dimer species with low volatility have already been detected on chamber experiments (Stolzenburg et al., 2018; Ye et al., 2019; Schervish and Donahue, 2020), they did not provide the explicit chemical kinetics of related reactions (i.e., the intermediate products and their yields), so it is hard to incorporate these reactions and species into the model. On the other hand, although yields of accretion products vary by 1 to 2 orders of magnitude in previous studies (Rissanen et al., 2015; Berndt et al., 2018; Zhao et al., 2018), the yields of C15 and C20 currently used are very low (4 %), resulting in relatively low dimer concentrations. Even if they were all ELVOCs and ULVOCs, it would not lead to a significant overestimation and, therefore, would not substantially impact nucleation and growth rates.

Neglecting the oligomerization and decomposition of accretion products may affect their concentrations; however, these effects are negligible. Not accounting for the oligomerization can lead to higher volatility of aerosols, resulting in a reduction of the mass concentration in the particle phase and condensation sink (CS) but increased mass in the gaseous phase. This could lead to an overestimation of the NPF rate. Since the mass of HOM-derived secondary organic aerosol (SOA) accounts for only about 10 % of the total SOA mass, the impact on NPF rate can be neglected. Not considering decomposition may result in an overestimation of the mass and number concentration of HOMs in the particle phase and consequently an overestimation of CS and an underestimation of the NPF rate. However, C15-SOA and C20-SOA account for less than 4 % of the total SOA (Liu et al., 2024), so this impact is also negligible.

We only implemented biogenic HOM chemistry in the global model due to the limited knowledge of explicit chemical reactions forming anthropogenic-derived HOMs (Wang et al., 2017; Wang et al., 2020; Garmash et al., 2020; Molteni et al., 2018). This treatment likely leads to an underestimation of organic nucleation rates, particularly in urban areas (Fig. 1). More studies on chemical mechanisms of anthropogenic HOMs which could be applied in global model are needed. Our findings suggest that subsequent growth of the newly formed particles to larger sizes may have a more significant effect on aerosol number than nucleation. More studies are needed to quantify the contribution of anthropogenic organics to the initial growth rate. Changes in simulated aerosol number and size distribution caused by anthropogenic HOMs-driven NPF can have important implications

for CCN concentrations and aerosol indirect forcing (Wang and Penner, 2009; Wang et al., 2009; Gordon et al., 2016; Zhu et al., 2019) and also need further analysis.

Besides organic species, the concentration of inorganic nucleating species will also affect the accuracy of the total nucleation rate. The overestimation of H_2SO_4 in CAM6-Chem could potentially impact our final results regarding the organic proportion in both nucleation and the initial growth rate because the dependencies of both the inorganic and organic nucleation rate on H_2SO_4 concentration are modeled with an exponent greater than 2 (Eqs. 2–6). Also, ammonia (NH_3) emissions used in this study are adapted from the Community Emissions Data System (CEDS), and they remain challenging to represent in models due to uncertainties, particularly in specific sectors. NH_3 emissions from human waste were adapted using methodologies from the Regional Emissions Inventory in Asia (REAS) (Kurokawa et al., 2013) and rely on a single global default emission factor. Not only is this emission factor uncertain, but also there will certainly be regional variations due to differing environmental conditions that we were unable to take into account (Hoesly et al., 2018). For agricultural emissions, the actual practices of managing livestock manure will affect true emissions; such practices vary significantly across the world but are not always well understood or reflected in the emission factors used in global inventories (Paulot et al., 2014). The aforementioned uncertainties in NH_3 will affect the inorganic nucleation rate and, consequently, the contribution of organics to the total nucleation rate.

In addition to the concentration of nucleating species, the uncertainty associated with NPF parameterization is also present in the model. Zhang et al. (2011) showed that radon contributes additional ionization in the boundary layer, especially over land. This implies that our pure organic nucleation rate might be underestimated since we only consider ion-pair production rate caused by galactic cosmic rays. This effect is negligible even over the continents since the contribution of ionization rate caused by the radioactive decay of radon is only significant ($> 30\%$) within the lowest 1 km (Fig. 12 in Zhang et al., 2011). Above 3 km, the contribution of radon-decay-induced ionization rate can be neglected ($< 10\%$). In this study, we focused on the proportion of organic NPF in the vertical integration within the whole atmosphere. Therefore, we will not consider incorporating the ion nucleation rate caused by radon.

The NPF rate at around 20 nm is calculated based on Eq. (14) from Kerminen and Kulmala (2002). This calculation is derived using several simplifying assumptions and approximations: (1) the only important sink for the newly formed particles is their coagulation with larger pre-existing particles, (2) the newly formed particles grow by condensation at a constant rate, and (3) the pre-existing population of larger particles remains unchanged during the growth of the newly formed particles. However, Lehtinen et al. (2007) reformulated the previously published theory (Kerminen and

Kulmala, 2002) to better account for the size dependence of the loss rates of newly formed particles (i.e., coagulation sink), rather than simplifying it as the gas condensation sink (CS). The uncertainty range caused by using the constant CS to replace the size-dependent coagulation sink (CoagS) is shown in Sect. S5. Recent studies (Stolzenburg et al., 2020; Ozon et al., 2021; Deng et al., 2020) also show that aerosol growth rates are not constant with size. However, CAM6-Chem does not include a nucleation mode, which means that newly formed particles grow from 1.7 to 20 nm (geometric diameter in Aitken mode) within one physical time step (30 min), making it impossible to resolve the growth rates of sub-20 nm particles. Future work, such as implementing a nucleation mode in CAM6-Chem and resolving particle growth rate within 20 nm, is therefore worth exploring.

References

Andreae, M. O.: Particle number concentrations measured by CPC and UHSAS during the ACRIDICON-CHUVA campaign in 2014, aircraft HALO database [data set], https://halo-db.pa.op.dlr.de/mission/5 (last access: 3 October 2020), 2020.

Andreae, M. O., Afchine, A., Albrecht, R., Holanda, B. A., Artaxo, P., Barbosa, H. M. J., Borrmann, S., Cecchini, M. A., Costa, A., Dollner, M., Fütterer, D., Järvinen, E., Jurkat, T., Klimach, T., Konemann, T., Knote, C., Krämer, M., Krisna, T., Machado, L. A. T., Mertes, S., Minikin, A., Pöhlker, C., Pöhlker, M. L., Pöschl, U., Rosenfeld, D., Sauer, D., Schlager, H., Schnaiter, M., Schneider, J., Schulz, C., Spanu, A., Sperling, V. B., Voigt, C., Walser, A., Wang, J., Weinzierl, B., Wendisch, M., and Ziereis, H.: Aerosol characteristics and particle production in the upper troposphere over the Amazon Basin, Atmos. Chem. Phys., 18, 921–961, https://doi.org/10.5194/acp-18-921-2018, 2018.

Andreae, M. O., Andreae, T. W., Ditas, F., and Pöhlker, C.: Frequent new particle formation at remote sites in the subboreal forest of North America, Atmos. Chem. Phys., 22, 2487–2505, https://doi.org/10.5194/acp-22-2487-2022, 2022.

Asmi, A., Wiedensohler, A., Laj, P., Fjaeraa, A.-M., Sellegri, K., Birmili, W., Weingartner, E., Baltensperger, U., Zdimal, V., Zikova, N., Putaud, J.-P., Marinoni, A., Tunved, P., Hansson, H.-C., Fiebig, M., Kivekäs, N., Lihavainen, H., Asmi, E., Ulevicius, V., Aalto, P. P., Swietlicki, E., Kristensson, A., Mihalopoulos, N., Kalivitis, N., Kalapov, I., Kiss, G., de Leeuw, G., Henzing, B., Harrison, R. M., Beddows, D., O'Dowd, C., Jennings, S. G., Flentje, H., Weinhold, K., Meinhardt, F., Ries, L., and Kulmala, M.: Number size distributions and seasonality of submicron particles in Europe 2008–2009, Atmos. Chem. Phys., 11, 5505–5538, https://doi.org/10.5194/acp-11-5505-2011, 2011.

Bellouin, N., Quaas, J., Gryspeerdt, E., Kinne, S., Stier, P., Watson-Parris, D., Boucher, O., Carslaw, K. S., Christensen, M., Daniau, A. L., Dufresne, J. L., Feingold, G., Fiedler, S., Forster, P., Gettelman, A., Haywood, J. M., Lohmann, U., Malavelle, F., Mauritsen, T., McCoy, D. T., Myhre, G., Mulmenstadt, J., Neubauer, D., Possner, A., Rugenstein, M., Sato, Y., Schulz, M., Schwartz, S. E., Sourdeval, O., Storelvmo, T., Toll, V., Winker,

D., and Stevens, B.: Bounding Global Aerosol Radiative Forcing of Climate Change, Rev. Geophys., 58, e2019RG000660, https://doi.org/10.1029/2019RG000660, 2020.

Berndt, T., Mentler, B., Scholz, W., Fischer, L., Herrmann, H., Kulmala, M., and Hansel, A.: Accretion Product Formation from Ozonolysis and OH Radical Reaction of á-Pinene: Mechanistic Insight and the Influence of Isoprene and Ethylene, Environ. Sci. Technol., 52, 11069–11077, https://doi.org/10.1021/acs.est.8b02210, 2018.

Bianchi, F., Trostl, J., Junninen, H., Frege, C., Henne, S., Hoyle, C. R., Molteni, U., Herrmann, E., Adamov, A., Bukowiecki, N., Chen, X., Duplissy, J., Gysel, M., Hutterli, M., Kangasluoma, J., Kontkanen, J., Kurten, A., Manninen, H. E., Munch, S., Perakyla, O., Petaja, T., Rondo, L., Williamson, C., Weingartner, E., Curtius, J., Worsnop, D. R., Kulmala, M., Dommen, J., and Baltensperger, U.: New particle formation in the free troposphere: A question of chemistry and timing, Science, 352, 1109–1112, https://doi.org/10.1126/science.aad5456, 2016.

Bianchi, F., Kurten, T., Riva, M., Mohr, C., Rissanen, M. P., Roldin, P., Berndt, T., Crounse, J. D., Wennberg, P. O., Mentel, T. F., Wildt, J., Junninen, H., Jokinen, T., Kulmala, M., Worsnop, D. R., Thornton, J. A., Donahue, N., Kjaergaard, H. G., and Ehn, M.: Highly Oxygenated Organic Molecules (HOM) from Gas-Phase Autoxidation Involving Peroxy Radicals: A Key Contributor to Atmospheric Aerosol, Chem. Rev., 119, 3472–3509, https://doi.org/10.1021/acs.chemrev.8b00395, 2019.

Boy, M., Karl, T., Turnipseed, A., Mauldin, R. L., Kosciuch, E., Greenberg, J., Rathbone, J., Smith, J., Held, A., Barsanti, K., Wehner, B., Bauer, S., Wiedensohler, A., Bonn, B., Kulmala, M., and Guenther, A.: New particle formation in the Front Range of the Colorado Rocky Mountains, Atmos. Chem. Phys., 8, 1577–1590, https://doi.org/10.5194/acp-8-1577-2008, 2008.

Carslaw, K. S.: Chapter 2 – Aerosol in the climate system, in: Aerosols and Climate, edited by: Carslaw, K. S., Elsevier, https://doi.org/10.1016/B978-0-12-819766-0.00008-0, 9–52, 2022.

Carslaw, K. S., Lee, L. A., Reddington, C. L., Pringle, K. J., Rap, A., Forster, P. M., Mann, G. W., Spracklen, D. V., Woodhouse, M. T., Regayre, L. A., and Pierce, J. R.: Large contribution of natural aerosols to uncertainty in indirect forcing, Nature, 503, 67–71, https://doi.org/10.1038/nature12674, 2013.

Deng, C. J., Fu, Y. Y., Dada, L., Yan, C., Cai, R. L., Yang, D. S., Zhou, Y., Yin, R. J., Lu, Y. Q., Li, X. X., Qiao, X. H., Fan, X. L., Nie, W., Kontkanen, J., Kangasluoma, J., Chu, B. W., Ding, A. J., Kerminen, V. M., Paasonen, P., Worsnop, D. R., Bianchi, F., Liu, Y. C., Zheng, J., Wang, L., Kulmala, M., and Jiang, J. K.: Seasonal Characteristics of New Particle Formation and Growth in Urban Beijing, Environ. Sci. Technol., 54, 8547–8557, https://doi.org/10.1021/acs.est.0c00808, 2020.

Dentener, F., Kinne, S., Bond, T., Boucher, O., Cofala, J., Generoso, S., Ginoux, P., Gong, S., Hoelzemann, J. J., Ito, A., Marelli, L., Penner, J. E., Putaud, J.-P., Textor, C., Schulz, M., van der Werf, G. R., and Wilson, J.: Emissions of primary aerosol and precursor gases in the years 2000 and 1750 prescribed data-sets for AeroCom, Atmos. Chem. Phys., 6, 4321–4344, https://doi.org/10.5194/acp-6-4321-2006, 2006.

Dunne, E. M., Gordon, H., Kurten, A., Almeida, J., Duplissy, J., Williamson, C., Ortega, I. K., Pringle, K. J., Adamov, A., Baltensperger, U., Barmet, P., Benduhn, F., Bianchi, F., Breit-

enlechner, M., Clarke, A., Curtius, J., Dommen, J., Donahue, N. M., Ehrhart, S., Flagan, R. C., Franchin, A., Guida, R., Hakala, J., Hansel, A., Heinritzi, M., Jokinen, T., Kangasluoma, J., Kirkby, J., Kulmala, M., Kupc, A., Lawler, M. J., Lehtipalo, K., Makhmutov, V., Mann, G., Mathot, S., Merikanto, J., Miettinen, P., Nenes, A., Onnela, A., Rap, A., Reddington, C. L. S., Riccobono, F., Richards, N. A. D., Rissanen, M. P., Rondo, L., Sarnela, N., Schobesberger, S., Sengupta, K., Simon, M., Sipilaa, M., Smith, J. N., Stozhkov, Y., Tome, A., Trostl, J., Wagner, P. E., Wimmer, D., Winkler, P. M., Worsnop, D. R., and Carslaw, K. S.: Global atmospheric particle formation from CERN CLOUD measurements, Science, 354, 1119–1124, https://doi.org/10.1126/science.aaf2649, 2016.

Ehn, M., Thornton, J. A., Kleist, E., Sipila, M., Junninen, H., Pullinen, I., Springer, M., Rubach, F., Tillmann, R., Lee, B., Lopez-Hilfiker, F., Andres, S., Acir, I. H., Rissanen, M., Jokinen, T., Schobesberger, S., Kangasluoma, J., Kontkanen, J., Nieminen, T., Kurten, T., Nielsen, L. B., Jorgensen, S., Kjaergaard, H. G., Canagaratna, M., Dal Maso, M., Berndt, T., Petaja, T., Wahner, A., Kerminen, V. M., Kulmala, M., Worsnop, D. R., Wildt, J., and Mentel, T. F.: A large source of low-volatility secondary organic aerosol, Nature, 506, 476–479, https://doi.org/10.1038/nature13032, 2014.

Emmons, L. K., Schwantes, R. H., Orlando, J. J., Tyndall, G., Kinnison, D., Lamarque, J. F., Marsh, D., Mills, M. J., Tilmes, S., Bardeen, C., Buchholz, R. R., Conley, A., Gettelman, A., Garcia, R., Simpson, I., Blake, D. R., Meinardi, S., and Pétron, G.: The Chemistry Mechanism in the Community Earth System Model Version 2 (CESM2), J. Adv. Model. Earth Sy., 12, e2019MS001882, https://doi.org/10.1029/2019ms001882, 2020.

Frege, C., Ortega, I. K., Rissanen, M. P., Praplan, A. P., Steiner, G., Heinritzi, M., Ahonen, L., Amorim, A., Bernhammer, A.-K., Bianchi, F., Brilke, S., Breitenlechner, M., Dada, L., Dias, A., Duplissy, J., Ehrhart, S., El-Haddad, I., Fischer, L., Fuchs, C., Garmash, O., Gonin, M., Hansel, A., Hoyle, C. R., Jokinen, T., Junninen, H., Kirkby, J., Kürten, A., Lehtipalo, K., Leiminger, M., Mauldin, R. L., Molteni, U., Nichman, L., Petäjä, T., Sarnela, N., Schobesberger, S., Simon, M., Sipilä, M., Stolzenburg, D., Tomé, A., Vogel, A. L., Wagner, A. C., Wagner, R., Xiao, M., Yan, C., Ye, P., Curtius, J., Donahue, N. M., Flagan, R. C., Kulmala, M., Worsnop, D. R., Winkler, P. M., Dommen, J., and Baltensperger, U.: Influence of temperature on the molecular composition of ions and charged clusters during pure biogenic nucleation, Atmos. Chem. Phys., 18, 65–79, https://doi.org/10.5194/acp-18-65-2018, 2018.

Garmash, O., Rissanen, M. P., Pullinen, I., Schmitt, S., Kausiala, O., Tillmann, R., Zhao, D., Percival, C., Bannan, T. J., Priestley, M., Hallquist, Å. M., Kleist, E., Kiendler-Scharr, A., Hallquist, M., Berndt, T., McFiggans, G., Wildt, J., Mentel, T. F., and Ehn, M.: Multi-generation OH oxidation as a source for highly oxygenated organic molecules from aromatics, Atmos. Chem. Phys., 20, 515–537, https://doi.org/10.5194/acp-20-515-2020, 2020.

Gordon, H., Sengupta, K., Rap, A., Duplissy, J., Frege, C., Williamson, C., Heinritzi, M., Simon, M., Yan, C., Almeida, J., Trostl, J., Nieminen, T., Ortega, I. K., Wagner, R., Dunne, E. M., Adamov, A., Amorim, A., Bernhammer, A. K., Bianchi, F., Breitenlechner, M., Brilke, S., Chen, X. M., Craven, J. S., Dias, A., Ehrhart, S., Fischer, L., Flagan, R. C., Franchin, A., Fuchs, C., Guida, R., Hakala, J., Hoyle, C. R., Jokinen, T., Junni-

nen, H., Kangasluoma, J., Kim, J., Kirkby, J., Krapf, M., Kurten, A., Laaksonen, A., Lehtipalo, K., Makhmutov, V., Mathot, S., Molteni, U., Monks, S. A., Onnela, A., Perakyla, O., Piel, F., Petaja, T., Praplanh, A. P., Pringle, K. J., Richards, N. A. D., Rissanen, M. P., Rondo, L., Sarnela, N., Schobesberger, S., Scott, C. E., Seinfeldo, J. H., Sharma, S., Sipila, M., Steiner, G., Stozhkov, Y., Stratmann, F., Tome, A., Virtanen, A., Vogel, A. L., Wagner, A. C., Wagner, P. E., Weingartner, E., Wimmer, D., Winkler, P. M., Ye, P. L., Zhang, X., Hansel, A., Dommen, J., Donahue, N. M., Worsnop, D. R., Baltensperger, U., Kulmala, M., Curtius, J., and Carslaw, K. S.: Reduced anthropogenic aerosol radiative forcing caused by biogenic new particle formation, P. Natl. Acad. Sci. USA, 113, 12053–12058, https://doi.org/10.1073/pnas.1602360113, 2016.

Gordon, H., Kirkby, J., Baltensperger, U., Bianchi, F., Breitenlechner, M., Curtius, J., Dias, A., Dommen, J., Donahue, N. M., Dunne, E. M., Duplissy, J., Ehrhart, S., Flagan, R. C., Frege, C., Fuchs, C., Hansel, A., Hoyle, C. R., Kulmala, M., Kurten, A., Lehtipalo, K., Makhmutov, V., Molteni, U., Rissanen, M. P., Stozhkov, Y., Trostl, J., Tsagkogeorgas, G., Wagner, R., Williamson, C., Wimmer, D., Winkler, P. M., Yan, C., and Carslaw, K. S.: Causes and importance of new particle formation in the present-day and preindustrial atmospheres, J. Geophys. Res.-Atmos., 122, 8739–8760, https://doi.org/10.1002/2017jd026844, 2017.

Guenther, A. B., Jiang, X., Heald, C. L., Sakulyanontvittaya, T., Duhl, T., Emmons, L. K., and Wang, X.: The Model of Emissions of Gases and Aerosols from Nature version 2.1 (MEGAN2.1): an extended and updated framework for modeling biogenic emissions, Geosci. Model Dev., 5, 1471–1492, https://doi.org/10.5194/gmd-5-1471-2012, 2012.

Heinritzi, M., Dada, L., Simon, M., Stolzenburg, D., Wagner, A. C., Fischer, L., Ahonen, L. R., Amanatidis, S., Baalbaki, R., Baccarini, A., Bauer, P. S., Baumgartner, B., Bianchi, F., Brilke, S., Chen, D., Chiu, R., Dias, A., Dommen, J., Duplissy, J., Finkenzeller, H., Frege, C., Fuchs, C., Garmash, O., Gordon, H., Granzin, M., El Haddad, I., He, X., Helm, J., Hofbauer, V., Hoyle, C. R., Kangasluoma, J., Keber, T., Kim, C., Kürten, A., Lamkaddam, H., Laurila, T. M., Lampilahti, J., Lee, C. P., Lehtipalo, K., Leiminger, M., Mai, H., Makhmutov, V., Manninen, H. E., Marten, R., Mathot, S., Mauldin, R. L., Mentler, B., Molteni, U., Müller, T., Nie, W., Nieminen, T., Onnela, A., Partoll, E., Passananti, M., Petäjä, T., Pfeifer, J., Pospisilova, V., Quéléver, L. L. J., Rissanen, M. P., Rose, C., Schobesberger, S., Scholz, W., Scholze, K., Sipilä, M., Steiner, G., Stozhkov, Y., Tauber, C., Tham, Y. J., Vazquez-Pufleau, M., Virtanen, A., Vogel, A. L., Volkamer, R., Wagner, R., Wang, M., Weitz, L., Wimmer, D., Xiao, M., Yan, C., Ye, P., Zha, Q., Zhou, X., Amorim, A., Baltensperger, U., Hansel, A., Kulmala, M., Tomé, A., Winkler, P. M., Worsnop, D. R., Donahue, N. M., Kirkby, J., and Curtius, J.: Molecular understanding of the suppression of new-particle formation by isoprene, Atmos. Chem. Phys., 20, 11809–11821, https://doi.org/10.5194/acp-20-11809-2020, 2020.

Hoesly, R. M., Smith, S. J., Feng, L., Klimont, Z., Janssens-Maenhout, G., Pitkanen, T., Seibert, J. J., Vu, L., Andres, R. J., Bolt, R. M., Bond, T. C., Dawidowski, L., Kholod, N., Kurokawa, J.-I., Li, M., Liu, L., Lu, Z., Moura, M. C. P., O'Rourke, P. R., and Zhang, Q.: Historical (1750–2014) anthropogenic emissions of reactive gases and aerosols from the Com-

munity Emissions Data System (CEDS), Geosci. Model Dev., 11, 369–408, https://doi.org/10.5194/gmd-11-369-2018, 2018.

Jo, D. S., Hodzic, A., Emmons, L. K., Marais, E. A., Peng, Z., Nault, B. A., Hu, W., Campuzano-Jost, P., and Jimenez, J. L.: A simplified parameterization of isoprene-epoxydiol-derived secondary organic aerosol (IEPOX-SOA) for global chemistry and climate models: a case study with GEOS-Chem v11-02-rc, Geosci. Model Dev., 12, 2983–3000, https://doi.org/10.5194/gmd-12-2983-2019, 2019.

Jo, D. S., Hodzic, A., Emmons, L. K., Tilmes, S., Schwantes, R. H., Mills, M. J., Campuzano-Jost, P., Hu, W., Zaveri, R. A., Easter, R. C., Singh, B., Lu, Z., Schulz, C., Schneider, J., Shilling, J. E., Wisthaler, A., and Jimenez, J. L.: Future changes in isoprene-epoxydiol-derived secondary organic aerosol (IEPOX SOA) under the Shared Socioeconomic Pathways: the importance of physicochemical dependency, Atmos. Chem. Phys., 21, 3395–3425, https://doi.org/10.5194/acp-21-3395-2021, 2021.

Jokinen, T., Berndt, T., Makkonen, R., Kerminen, V. M., Junninen, H., Paasonen, P., Stratmann, F., Herrmann, H., Guenther, A. B., Worsnop, D. R., Kulmala, M., Ehn, M., and Sipila, M.: Production of extremely low volatile organic compounds from biogenic emissions: Measured yields and atmospheric implications, P. Natl. Acad. Sci. USA, 112, 7123–7128, https://doi.org/10.1073/pnas.1423977112, 2015.

Kerminen, V. M. and Kulmala, M.: Analytical formulae connecting the "real" and the "apparent" nucleation rate and the nuclei number concentration for atmospheric nucleation events, J. Atmos. Sci., 33, 609–622, https://doi.org/10.1016/s0021-8502(01)00194-x, 2002.

Kerminen, V. M., Chen, X. M., Vakkari, V., Petaja, T., Kulmala, M., and Bianchi, F.: Atmospheric new particle formation and growth: review of field observations, Environ. Res. Lett., 13, 103003, https://doi.org/10.1088/1748-9326/aadf3c, 2018.

Kirkby, J., Duplissy, J., Sengupta, K., Frege, C., Gordon, H., Williamson, C., Heinritzi, M., Simon, M., Yan, C., Almeida, J., Trostl, J., Nieminen, T., Ortega, I. K., Wagner, R., Adamov, A., Amorim, A., Bernhammer, A. K., Bianchi, F., Breitenlechner, M., Brilke, S., Chen, X. M., Craven, J., Dias, A., Ehrhart, S., Flagan, R. C., Franchin, A., Fuchs, C., Guida, R., Hakala, J., Hoyle, C. R., Jokinen, T., Junninen, H., Kangasluoma, J., Kim, J., Krapf, M., Kurten, A., Laaksonen, A., Lehtipalo, K., Makhmutov, V., Mathot, S., Molteni, U., Onnela, A., Perakyla, O., Piel, F., Petaja, T., Praplan, A. P., Pringle, K., Rap, A., Richards, N. A. D., Riipinen, I., Rissanen, M. P., Rondo, L., Sarnela, N., Schobesberger, S., Scott, C. E., Seinfeld, J. H., Sipila, M., Steiner, G., Stozhkov, Y., Stratmann, F., Tome, A., Virtanen, A., Vogel, A. L., Wagner, A. C., Wagner, P. E., Weingartner, E., Wimmer, D., Winkler, P. M., Ye, P. L., Zhang, X., Hansel, A., Dommen, J., Donahue, N. M., Worsnop, D. R., Baltensperger, U., Kulmala, M., Carslaw, K. S., and Curtius, J.: Ion-induced nucleation of pure biogenic particles, Nature, 533, 521–526, https://doi.org/10.1038/nature17953, 2016.

Kooperman, G. J., Pritchard, M. S., Ghan, S. J., Wang, M., Somerville, R. C. J., and Russell, L. M.: Constraining the influence of natural variability to improve estimates of global aerosol indirect effects in a nudged version of the Community Atmosphere Model 5, J. Geophys. Res.-Atmos., 117, D23204, https://doi.org/10.1029/2012jd018588, 2012.

Krapf, M., El Haddad, I., Bruns, Emily A., Molteni, U., Daellenbach, Kaspar R., Prévôt, André S. H., Baltensperger, U., and Dommen, J.: Labile Peroxides in Secondary Organic Aerosol, Chem, 1, 603–616, https://doi.org/10.1016/j.chempr.2016.09.007, 2016.

Kuang, C., McMurry, P. H., McCormick, A. V., and Eisele, F. L.: Dependence of nucleation rates on sulfuric acid vapor concentration in diverse atmospheric locations, J. Geophys. Res.-Atmos., 113, D10209, https://doi.org/10.1029/2007jd009253, 2008.

Kulmala, M.: How Particles Nucleate and Grow, Science, 302, 1000–1001, https://doi.org/10.1126/science.1090848, 2003.

Kulmala, M., Lehtinen, K. E. J., and Laaksonen, A.: Cluster activation theory as an explanation of the linear dependence between formation rate of 3nm particles and sulphuric acid concentration, Atmos. Chem. Phys., 6, 787–793, https://doi.org/10.5194/acp-6-787-2006, 2006.

Kulmala, M., Asmi, A., Lappalainen, H. K., Carslaw, K. S., Pöschl, U., Baltensperger, U., Hov, Ø., Brenquier, J.-L., Pandis, S. N., Facchini, M. C., Hansson, H.-C., Wiedensohler, A., and O'Dowd, C. D.: Introduction: European Integrated Project on Aerosol Cloud Climate and Air Quality interactions (EUCAARI) – integrating aerosol research from nano to global scales, Atmos. Chem. Phys., 9, 2825–2841, https://doi.org/10.5194/acp-9-2825-2009, 2009.

Kurokawa, J., Ohara, T., Morikawa, T., Hanayama, S., Janssens-Maenhout, G., Fukui, T., Kawashima, K., and Akimoto, H.: Emissions of air pollutants and greenhouse gases over Asian regions during 2000–2008: Regional Emission inventory in ASia (REAS) version 2, Atmos. Chem. Phys., 13, 11019–11058, https://doi.org/10.5194/acp-13-11019-2013, 2013.

Kurtén, T., Tiusanen, K., Roldin, P., Rissanen, M., Luy, J.-N., Boy, M., Ehn, M., and Donahue, N.: α-Pinene Autoxidation Products May Not Have Extremely Low Saturation Vapor Pressures Despite High O : C Ratios, J. Phys. Chem. A, 120, 2569–2582, https://doi.org/10.1021/acs.jpca.6b02196, 2016

Lee, S., Shin, J. E., Yoon, R., Yoo, H., and Kim, S.: Annulation of O-silyl N,O-ketene acetals with alkynes for the synthesis of dihydropyridinones and its application in concise total synthesis of phenanthroindolizidine alkaloids, Front. Chem., 11, 1267422, https://doi.org/10.3389/fchem.2023.1267422, 2023.

Lehtinen, K. E. J., Dal Maso, M., Kulmala, M., and Kerminen, V.-M.: Estimating nucleation rates from apparent particle formation rates and vice versa: Revised formulation of the Kerminen–Kulmala equation, J. Aerosol Sci., 38, 988–994, https://doi.org/10.1016/j.jaerosci.2007.06.009, 2007.

Li, M., Liu, H., Geng, G., Hong, C., Liu, F., Song, Y., Tong, D., Zheng, B., Cui, H., Man, H., Zhang, Q., and He, K.: Anthropogenic emission inventories in China: a review, Natl. Sci. Rev., 4, 834–866, https://doi.org/10.1093/nsr/nwx150, 2017.

Liu, X., Ma, P.-L., Wang, H., Tilmes, S., Singh, B., Easter, R. C., Ghan, S. J., and Rasch, P. J.: Description and evaluation of a new four-mode version of the Modal Aerosol Module (MAM4) within version 5.3 of the Community Atmosphere Model, Geosci. Model Dev., 9, 505–522, https://doi.org/10.5194/gmd-9-505-2016, 2016.

Liu, Y., Dong, X., Emmons, L. K., Jo, D. S., Liu, Y., Shrivastava, M., Yue, M., Liang, Y., Song, Z., He, X., and Wang, M.: Exploring the Factors Controlling the Long-Term Trend (1988–2019) of Surface Organic Aerosols in the Continental United States

by Simulations, J. Geophys. Res.-Atmos., 128, e2022JD037935, https://doi.org/10.1029/2022jd037935, 2023.

Liu, Y., Dong, X., Wang, M., Xu, R., Thornton, J. A., Shao, X., Emmons, L. K., Jo, D. S., Yue, M., and Shrivastava, M.: A Modeling Study of Global Distribution and Formation Pathways of Highly Oxygenated Organic Molecules Derived Secondary Organic Aerosols (HOMs-SOA) from Monoterpenes, Geosci. Model Dev., in preparation, 2024.

Luo, Z., Zhang, Y., Chen, W., Van Damme, M., Coheur, P.-F., and Clarisse, L.: Estimating global ammonia (NH_3) emissions based on IASI observations from 2008 to 2018, Atmos. Chem. Phys., 22, 10375–10388, https://doi.org/10.5194/acp-22-10375-2022, 2022.

Mann, G. W., Carslaw, K. S., Reddington, C. L., Pringle, K. J., Schulz, M., Asmi, A., Spracklen, D. V., Ridley, D. A., Woodhouse, M. T., Lee, L. A., Zhang, K., Ghan, S. J., Easter, R. C., Liu, X., Stier, P., Lee, Y. H., Adams, P. J., Tost, H., Lelieveld, J., Bauer, S. E., Tsigaridis, K., van Noije, T. P. C., Strunk, A., Vignati, E., Bellouin, N., Dalvi, M., Johnson, C. E., Bergman, T., Kokkola, H., von Salzen, K., Yu, F., Luo, G., Petzold, A., Heintzenberg, J., Clarke, A., Ogren, J. A., Gras, J., Baltensperger, U., Kaminski, U., Jennings, S. G., O'Dowd, C. D., Harrison, R. M., Beddows, D. C. S., Kulmala, M., Viisanen, Y., Ulevicius, V., Mihalopoulos, N., Zdimal, V., Fiebig, M., Hansson, H.-C., Swietlicki, E., and Henzing, J. S.: Intercomparison and evaluation of global aerosol microphysical properties among AeroCom models of a range of complexity, Atmos. Chem. Phys., 14, 4679–4713, https://doi.org/10.5194/acp-14-4679-2014, 2014.

McMurry, P. H., Fink, M., Sakurai, H., Stolzenburg, M. R., Mauldin, R. L., Smith, J., Eisele, F., Moore, K., Sjostedt, S., Tanner, D., Huey, L. G., Nowak, J. B., Edgerton, E., and Voisin, D.: A criterion for new particle formation in the sulfur-rich Atlanta atmosphere, J. Geophys. Res.-Atmos., 110, D22S0, https://doi.org/10.1029/2005jd005901, 2005.

Merikanto, J., Napari, I., Vehkamaki, H., Anttila, T., and Kulmala, M.: New parameterization of sulfuric acid-ammonia-water ternary nucleation rates at tropospheric conditions, J. Geophys. Res.-Atmos., 112, D15207, https://doi.org/10.1029/2006jd007977, 2007.

Merikanto, J., Spracklen, D. V., Mann, G. W., Pickering, S. J., and Carslaw, K. S.: Impact of nucleation on global CCN, Atmos. Chem. Phys., 9, 8601–8616, https://doi.org/10.5194/acp-9-8601-2009, 2009.

Mohr, C., Thornton, J. A., Heitto, A., Lopez-Hilfiker, F. D., Lutz, A., Riipinen, I., Hong, J., Donahue, N. M., Hallquist, M., Petaja, T., Kulmala, M., and Yli-Juuti, T.: Molecular identification of organic vapors driving atmospheric nanoparticle growth, Nat. Commun., 10, 4442, https://doi.org/10.1038/s41467-019-12473-2, 2019.

Molteni, U., Bianchi, F., Klein, F., El Haddad, I., Frege, C., Rossi, M. J., Dommen, J., and Baltensperger, U.: Formation of highly oxygenated organic molecules from aromatic compounds, Atmos. Chem. Phys., 18, 1909–1921, https://doi.org/10.5194/acp-18-1909-2018, 2018.

Ozon, M., Stolzenburg, D., Dada, L., Seppänen, A., and Lehtinen, K. E. J.: Aerosol formation and growth rates from chamber experiments using Kalman smoothing, Atmos. Chem. Phys., 21, 12595–12611, https://doi.org/10.5194/acp-21-12595-2021, 2021.

Paasonen, P., Nieminen, T., Asmi, E., Manninen, H. E., Petäjä, T., Plass-Dülmer, C., Flentje, H., Birmili, W., Wiedensohler, A., Hõrrak, U., Metzger, A., Hamed, A., Laaksonen, A., Facchini, M. C., Kerminen, V.-M., and Kulmala, M.: On the roles of sulphuric acid and low-volatility organic vapours in the initial steps of atmospheric new particle formation, Atmos. Chem. Phys., 10, 11223–11242, https://doi.org/10.5194/acp-10-11223-2010, 2010.

Paulot, F., Jacob, D. J., Pinder, R. W., Bash, J. O., Travis, K., and Henze, D. K.: Ammonia emissions in the United States, European Union, and China derived by high-resolution inversion of ammonium wet deposition data: Interpretation with a new agricultural emissions inventory (MASAGE_NH3), J. Geophys. Res.-Atmos., 119, 4343–4364, https://doi.org/10.1002/2013JD021130, 2014.

Paulot, F., Paynter, D., Ginoux, P., Naik, V., and Horowitz, L. W.: Changes in the aerosol direct radiative forcing from 2001 to 2015: observational constraints and regional mechanisms, Atmos. Chem. Phys., 18, 13265–13281, https://doi.org/10.5194/acp-18-13265-2018, 2018.

Pierce, J. R. and Adams, P. J.: A Computationally Efficient Aerosol Nucleation/Condensation Method: Pseudo-Steady-State Sulfuric Acid, Aerosol Sci. Tech., 43, 216–226, https://doi.org/10.1080/02786820802587896, 2009.

Pye, H. O. T., D'Ambro, E. L., Lee, B. H., Schobesberger, S., Takeuchi, M., Zhao, Y., Lopez-Hilfiker, F., Liu, J., Shilling, J. E., Xing, J., Mathur, R., Middlebrook, A. M., Liao, J., Welti, A., Graus, M., Warneke, C., de Gouw, J. A., Holloway, J. S., Ryerson, T. B., Pollack, I. B., and Thornton, J. A.: Anthropogenic enhancements to production of highly oxygenated molecules from autoxidation, P. Natl. Acad. Sci. USA, 116, 6641–6646, https://doi.org/10.1073/pnas.1810774116, 2019.

Reddington, C. L., Carslaw, K. S., Stier, P., Schutgens, N., Coe, H., Liu, D., Allan, J., Browse, J., Pringle, K. J., Lee, L. A., Yoshioka, M., Johnson, J. S., Regayre, L. A., Spracklen, D. V., Mann, G. W., Clarke, A., Hermann, M., Henning, S., Wex, H., Kristensen, T. B., Leaitch, W. R., Pöschl, U., Rose, D., Andreae, M. O., Schmale, J., Kondo, Y., Oshima, N., Schwarz, J. P., Nenes, A., Anderson, B., Roberts, G. C., Snider, J. R., Leck, C., Quinn, P. K., Chi, X., Ding, A., Jimenez, J. L., and Zhang, Q.: The Global Aerosol Synthesis and Science Project (GASSP): Measurements and Modeling to Reduce Uncertainty, B. Am. Meteorol. Soc., 98, 1857–1877, https://doi.org/10.1175/bams-d-15-00317.1, 2017.

Riccobono, F., Schobesberger, S., Scott, C. E., Dommen, J., Ortega, I. K., Rondo, L., Almeida, J., Amorim, A., Bianchi, F., Breitenlechner, M., David, A., Downard, A., Dunne, E. M., Duplissy, J., Ehrhart, S., Flagan, R. C., Franchin, A., Hansel, A., Junninen, H., Kajos, M., Keskinen, H., Kupc, A., Kurten, A., Kvashin, A. N., Laaksonen, A., Lehtipalo, K., Makhmutov, V., Mathot, S., Nieminen, T., Onnela, A., Petaja, T., Praplan, A. P., Santos, F. D., Schallhart, S., Seinfeld, J. H., Sipila, M., Spracklen, D. V., Stozhkov, Y., Stratmann, F., Tome, A., Tsagkogeorgas, G., Vaattovaara, P., Viisanen, Y., Vrtala, A., Wagner, P. E., Weingartner, E., Wex, H., Wimmer, D., Carslaw, K. S., Curtius, J., Donahue, N. M., Kirkby, J., Kulmala, M., Worsnop, D. R., and Baltensperger, U.: Oxidation Products of Biogenic Emissions Contribute to Nucleation of Atmospheric Particles, Science, 344, 717–721, https://doi.org/10.1126/science.1243527, 2014.

Rissanen, M. P., Kurtén, T., Sipilä, M., Thornton, J. A., Kausiala, O., Garmash, O., Kjaergaard, H. G., Petäjä, T., Worsnop, D. R., Ehn, M., and Kulmala, M.: Effects of Chemical Complexity on the Autoxidation Mechanisms of Endocyclic Alkene Ozonolysis Products: From Methylcyclohexenes toward Understanding á-Pinene, J. Phys. Chem. A, 119, 4633–4650, https://doi.org/10.1021/jp510966g, 2015.

Roldin, P., Ehn, M., Kurtén, T., Olenius, T., Rissanen, M. P., Sarnela, N., Elm, J., Rantala, P., Hao, L., Hyttinen, N., Heikkinen, L., Worsnop, D. R., Pichelstorfer, L., Xavier, C., Clusius, P., Öström, E., Petäjä, T., Kulmala, M., Vehkamäki, H., Virtanen, A., Riipinen, I., and Boy, M.: The role of highly oxygenated organic molecules in the Boreal aerosol-cloud-climate system, Nat. Commun., 10, 4370, https://doi.org/10.1038/s41467-019-12338-8, 2019.

Rosenfeld, D., Lohmann, U., Raga, G. B., O'Dowd, C. D., Kulmala, M., Fuzzi, S., Reissell, A., and Andreae, M. O.: Flood or Drought: How Do Aerosols Affect Precipitation?, Science, 321, 1309–1313, https://doi.org/10.1126/science.1160606, 2008.

Rosenfeld, D., Andreae, M. O., Asmi, A., Chin, M., de Leeuw, G., Donovan, D. P., Kahn, R., Kinne, S., Kivekäs, N., Kulmala, M., Lau, W., Schmidt, K. S., Suni, T., Wagner, T., Wild, M., and Quaas, J.: Global observations of aerosol-cloud-precipitation-climate interactions, Rev. Geophys., 52, 750–808, https://doi.org/10.1002/2013rg000441, 2014.

Schervish, M. and Donahue, N. M.: Peroxy radical chemistry and the volatility basis set, Atmos. Chem. Phys., 20, 1183–1199, https://doi.org/10.5194/acp-20-1183-2020, 2020.

Scott, C. E., Rap, A., Spracklen, D. V., Forster, P. M., Carslaw, K. S., Mann, G. W., Pringle, K. J., Kivekäs, N., Kulmala, M., Lihavainen, H., and Tunved, P.: The direct and indirect radiative effects of biogenic secondary organic aerosol, Atmos. Chem. Phys., 14, 447–470, https://doi.org/10.5194/acp-14-447-2014, 2014.

Shiraiwa, M., Ueda, K., Pozzer, A., Lammel, G., Kampf, C. J., Fushimi, A., Enami, S., Arangio, A. M., Frohlich-Nowoisky, J., Fujitani, Y., Furuyama, A., Lakey, P. S. J., Lelieveld, J., Lucas, K., Morino, Y., Poschl, U., Takahama, S., Takami, A., Tong, H., Weber, B., Yoshino, A., and Sato, K.: Aerosol Health Effects from Molecular to Global Scales, Environ. Sci. Technol., 51, 13545–13567, https://doi.org/10.1021/acs.est.7b04417, 2017.

Sihto, S.-L., Kulmala, M., Kerminen, V.-M., Dal Maso, M., Petäjä, T., Riipinen, I., Korhonen, H., Arnold, F., Janson, R., Boy, M., Laaksonen, A., and Lehtinen, K. E. J.: Atmospheric sulphuric acid and aerosol formation: implications from atmospheric measurements for nucleation and early growth mechanisms, Atmos. Chem. Phys., 6, 4079–4091, https://doi.org/10.5194/acp-6-4079-2006, 2006.

Simon, M., Dada, L., Heinritzi, M., Scholz, W., Stolzenburg, D., Fischer, L., Wagner, A. C., Kürten, A., Rörup, B., He, X.-C., Almeida, J., Baalbaki, R., Baccarini, A., Bauer, P. S., Beck, L., Bergen, A., Bianchi, F., Bräkling, S., Brilke, S., Caudillo, L., Chen, D., Chu, B., Dias, A., Draper, D. C., Duplissy, J., El-Haddad, I., Finkenzeller, H., Frege, C., Gonzalez-Carracedo, L., Gordon, H., Granzin, M., Hakala, J., Hofbauer, V., Hoyle, C. R., Kim, C., Kong, W., Lamkaddam, H., Lee, C. P., Lehtipalo, K., Leiminger, M., Mai, H., Manninen, H. E., Marie, G., Marten, R., Mentler, B., Molteni, U., Nichman, L., Nie, W., Ojdanic, A., Onnela, A., Partoll, E., Petäjä, T., Pfeifer, J., Philip-

pov, M., Quéléver, L. L. J., Ranjithkumar, A., Rissanen, M. P., Schallhart, S., Schobesberger, S., Schuchmann, S., Shen, J., Sipilä, M., Steiner, G., Stozhkov, Y., Tauber, C., Tham, Y. J., Tomé, A. R., Vazquez-Pufleau, M., Vogel, A. L., Wagner, R., Wang, M., Wang, D. S., Wang, Y., Weber, S. K., Wu, Y., Xiao, M., Yan, C., Ye, P., Ye, Q., Zauner-Wieczorek, M., Zhou, X., Baltensperger, U., Dommen, J., Flagan, R. C., Hansel, A., Kulmala, M., Volkamer, R., Winkler, P. M., Worsnop, D. R., Donahue, N. M., Kirkby, J., and Curtius, J.: Molecular understanding of new-particle formation from α-pinene between −50 and +25 °C, Atmos. Chem. Phys., 20, 9183–9207, https://doi.org/10.5194/acp-20-9183-2020, 2020.

Spracklen, D. V., Carslaw, K. S., Kulmala, M., Kerminen, V.-M., Mann, G. W., and Sihto, S.-L.: The contribution of boundary layer nucleation events to total particle concentrations on regional and global scales, Atmos. Chem. Phys., 6, 5631–5648, https://doi.org/10.5194/acp-6-5631-2006, 2006.

Spracklen, D. V., Carslaw, K. S., Merikanto, J., Mann, G. W., Reddington, C. L., Pickering, S., Ogren, J. A., Andrews, E., Baltensperger, U., Weingartner, E., Boy, M., Kulmala, M., Laakso, L., Lihavainen, H., Kivekäs, N., Komppula, M., Mihalopoulos, N., Kouvarakis, G., Jennings, S. G., O'Dowd, C., Birmili, W., Wiedensohler, A., Weller, R., Gras, J., Laj, P., Sellegri, K., Bonn, B., Krejci, R., Laaksonen, A., Hamed, A., Minikin, A., Harrison, R. M., Talbot, R., and Sun, J.: Explaining global surface aerosol number concentrations in terms of primary emissions and particle formation, Atmos. Chem. Phys., 10, 4775–4793, https://doi.org/10.5194/acp-10-4775-2010, 2010.

Stolzenburg, D., Fischer, L., Vogel, A. L., Heinritzi, M., Schervish, M., Simon, M., Wagner, A. C., Dada, L., Ahonen, L. R., Amorim, A., Baccarini, A., Bauer, P. S., Baumgartner, B., Bergen, A., Bianchi, F., Breitenlechner, M., Brilke, S., Buenrostro Mazon, S., Chen, D., Dias, A., Draper, D. C., Duplissy, J., El Haddad, I., Finkenzeller, H., Frege, C., Fuchs, C., Garmash, O., Gordon, H., He, X., Helm, J., Hofbauer, V., Hoyle, C. R., Kim, C., Kirkby, J., Kontkanen, J., Kürten, A., Lampilahti, J., Lawler, M., Lehtipalo, K., Leiminger, M., Mai, H., Mathot, S., Mentler, B., Molteni, U., Nie, W., Nieminen, T., Nowak, J. B., Ojdanic, A., Onnela, A., Passananti, M., Petäjä, T., Quéléver, L. L. J., Rissanen, M. P., Sarnela, N., Schallhart, S., Tauber, C., Tomé, A., Wagner, R., Wang, M., Weitz, L., Wimmer, D., Xiao, M., Yan, C., Ye, P., Zha, Q., Baltensperger, U., Curtius, J., Dommen, J., Flagan, R. C., Kulmala, M., Smith, J. N., Worsnop, D. R., Hansel, A., Donahue, N. M., and Winkler, P. M.: Rapid growth of organic aerosol nanoparticles over a wide tropospheric temperature range, P. Natl. Acad. Sci. USA, 115, 9122–9127, https://doi.org/10.1073/pnas.1807604115, 2018.

Stolzenburg, D., Simon, M., Ranjithkumar, A., Kürten, A., Lehtipalo, K., Gordon, H., Ehrhart, S., Finkenzeller, H., Pichelstorfer, L., Nieminen, T., He, X.-C., Brilke, S., Xiao, M., Amorim, A., Baalbaki, R., Baccarini, A., Beck, L., Bräkling, S., Caudillo Murillo, L., Chen, D., Chu, B., Dada, L., Dias, A., Dommen, J., Duplissy, J., El Haddad, I., Fischer, L., Gonzalez Carracedo, L., Heinritzi, M., Kim, C., Koenig, T. K., Kong, W., Lamkaddam, H., Lee, C. P., Leiminger, M., Li, Z., Makhmutov, V., Manninen, H. E., Marie, G., Marten, R., Müller, T., Nie, W., Partoll, E., Petäjä, T., Pfeifer, J., Philippov, M., Rissanen, M. P., Rörup, B., Schobesberger, S., Schuchmann, S., Shen, J., Sipilä, M., Steiner, G., Stozhkov, Y., Tauber, C., Tham, Y. J., Tomé, A., Vazquez-

Pufleau, M., Wagner, A. C., Wang, M., Wang, Y., Weber, S. K., Wimmer, D., Wlasits, P. J., Wu, Y., Ye, Q., Zauner-Wieczorek, M., Baltensperger, U., Carslaw, K. S., Curtius, J., Donahue, N. M., Flagan, R. C., Hansel, A., Kulmala, M., Lelieveld, J., Volkamer, R., Kirkby, J., and Winkler, P. M.: Enhanced growth rate of atmospheric particles from sulfuric acid, Atmos. Chem. Phys., 20, 7359–7372, https://doi.org/10.5194/acp-20-7359-2020, 2020.

Tröstl, J., Chuang, W. K., Gordon, H., Heinritzi, M., Yan, C., Molteni, U., Ahlm, L., Frege, C., Bianchi, F., Wagner, R., Simon, M., Lehtipalo, K., Williamson, C., Craven, J. S., Duplissy, J., Adamov, A., Almeida, J., Bernhammer, A. K., Breitenlechner, M., Brilke, S., Dias, A., Ehrhart, S., Flagan, R. C., Franchin, A., Fuchs, C., Guida, R., Gysel, M., Hansel, A., Hoyle, C. R., Jokinen, T., Junninen, H., Kangasluoma, J., Keskinen, H., Kim, J., Krapf, M., Kurten, A., Laaksonen, A., Lawler, M., Leiminger, M., Mathot, S., Mohler, O., Nieminen, T., Onnela, A., Petaja, T., Piel, F. M., Miettinen, P., Rissanen, M. P., Rondo, L., Sarnela, N., Schobesberger, S., Sengupta, K., Sipila, M., Smith, J. N., Steiner, G., Tome, A., Virtanen, A., Wagner, A. C., Weingartner, E., Wimmer, D., Winkler, P. M., Ye, P. L., Carslaw, K. S., Curtius, J., Dommen, J., Kirkby, J., Kulmala, M., Riipinen, I., Worsnop, D. R., Donahue, N. M., and Baltensperger, U.: The role of low-volatility organic compounds in initial particle growth in the atmosphere, Nature, 533, 527–531, https://doi.org/10.1038/nature18271, 2016.

van der Werf, G. R., Randerson, J. T., Giglio, L., van Leeuwen, T. T., Chen, Y., Rogers, B. M., Mu, M., van Marle, M. J. E., Morton, D. C., Collatz, G. J., Yokelson, R. J., and Kasibhatla, P. S.: Global fire emissions estimates during 1997–2016, Earth Syst. Sci. Data, 9, 697–720, https://doi.org/10.5194/essd-9-697-2017, 2017.

van Marle, M. J. E., Kloster, S., Magi, B. I., Marlon, J. R., Daniau, A.-L., Field, R. D., Arneth, A., Forrest, M., Hantson, S., Kehrwald, N. M., Knorr, W., Lasslop, G., Li, F., Mangeon, S., Yue, C., Kaiser, J. W., and van der Werf, G. R.: Historic global biomass burning emissions for CMIP6 (BB4CMIP) based on merging satellite observations with proxies and fire models (1750–2015), Geosci. Model Dev., 10, 3329–3357, https://doi.org/10.5194/gmd-10-3329-2017, 2017.

Vehkamaki, H., Kulmala, M., Napari, I., Lehtinen, K. E. J., Timmreck, C., Noppel, M., and Laaksonen, A.: An improved parameterization for sulfuric acid–water nucleation rates for tropospheric and stratospheric conditions, J. Geophys. Res.-Atmos., 107, AAC 3-1–AAC 3-10, https://doi.org/10.1029/2002jd002184, 2002.

Wang, M. and Penner, J. E.: Aerosol indirect forcing in a global model with particle nucleation, Atmos. Chem. Phys., 9, 239–260, https://doi.org/10.5194/acp-9-239-2009, 2009.

Wang, M., Penner, J. E., and Liu, X.: Coupled IMPACT aerosol and NCAR CAM3 model: Evaluation of predicted aerosol number and size distribution, J. Geophys. Res.-Atmos., 114, D06302, https://doi.org/10.1029/2008jd010459, 2009.

Wang, S. N., Wu, R. R., Berndt, T., Ehn, M., and Wang, L. M.: Formation of Highly Oxidized Radicals and Multifunctional Products from the Atmospheric Oxidation of Alkylbenzenes, Environ. Sci. Technol., 51, 8442–8449, https://doi.org/10.1021/acs.est.7b02374, 2017.

Wang, Y., Mehra, A., Krechmer, J. E., Yang, G., Hu, X., Lu, Y., Lambe, A., Canagaratna, M., Chen, J., Worsnop, D., Coe, H.,

and Wang, L.: Oxygenated products formed from OH-initiated reactions of trimethylbenzene: autoxidation and accretion, Atmos. Chem. Phys., 20, 9563–9579, https://doi.org/10.5194/acp-20-9563-2020, 2020.

Weber, J., Archer-Nicholls, S., Griffiths, P., Berndt, T., Jenkin, M., Gordon, H., Knote, C., and Archibald, A. T.: CRI-HOM: A novel chemical mechanism for simulating highly oxygenated organic molecules (HOMs) in global chemistry–aerosol–climate models, Atmos. Chem. Phys., 20, 10889–10910, https://doi.org/10.5194/acp-20-10889-2020, 2020.

Weber, R. J., Marti, J. J., McMurry, P. H., Eisele, F. L., Tanner, D. J., and Jefferson, A.: Measurements of new particle formation and ultrafine particle growth rates at a clean continental site, J. Geophys. Res.-Atmos., 102, 4375–4385, https://doi.org/10.1029/96jd03656, 1997.

Wendisch, M., Pöschl, U., Andreae, M. O., Machado, L. A. T., Albrecht, R., Schlager, H., Rosenfeld, D., Martin, S. T., Abdelmonem, A., Afchine, A., Araùjo, A. C., Artaxo, P., Aufmhoff, H., Barbosa, H. M. J., Borrmann, S., Braga, R., Buchholz, B., Cecchini, M. A., Costa, A., Curtius, J., Dollner, M., Dorf, M., Dreiling, V., Ebert, V., Ehrlich, A., Ewald, F., Fisch, G., Fix, A., Frank, F., Fütterer, D., Heckl, C., Heidelberg, F., Hüneke, T., Jäkel, E., Järvinen, E., Jurkat, T., Kanter, S., Kästner, U., Kenntner, M., Kesselmeier, J., Klimach, T., Knecht, M., Kohl, R., Kölling, T., Krämer, M., Krüger, M., Krisna, T. C., Lavric, J. V., Longo, K., Mahnke, C., Manzi, A. O., Mayer, B., Mertes, S., Minikin, A., Molleker, S., Münch, S., Nillius, B., Pfeilsticker, K., Pöhlker, C., Roiger, A., Rose, D., Rosenow, D., Sauer, D., Schnaiter, M., Schneider, J., Schulz, C., de Souza, R. A. F., Spanu, A., Stock, P., Vila, D., Voigt, C., Walser, A., Walter, D., Weigel, R., Weinzierl, B., Werner, F., Yamasoe, M. A., Ziereis, H., Zinner, T., and Zöger, M.: ACRIDICON–CHUVA Campaign: Studying Tropical Deep Convective Clouds and Precipitation over Amazonia Using the New German Research Aircraft HALO, B. Am. Meteorol. Soc., 97, 1885–1908, https://doi.org/10.1175/BAMS-D-14-00255.1, 2016.

Xu, L., Pye, H. O. T., He, J., Chen, Y., Murphy, B. N., and Ng, N. L.: Experimental and model estimates of the contributions from biogenic monoterpenes and sesquiterpenes to secondary organic aerosol in the southeastern United States, Atmos. Chem. Phys., 18, 12613–12637, https://doi.org/10.5194/acp-18-12613-2018, 2018.

Xu, R., Thornton, J. A., Lee, B. H., Zhang, Y., Jaeglé, L., Lopez-Hilfiker, F. D., Rantala, P., and Petäjä, T.: Global simulations of monoterpene-derived peroxy radical fates and the distributions of highly oxygenated organic molecules (HOMs) and accretion products, Atmos. Chem. Phys., 22, 5477–5494, https://doi.org/10.5194/acp-22-5477-2022, 2022.

Ye, Q., Wang, M., Hofbauer, V., Stolzenburg, D., Chen, D., Schervish, M., Vogel, A., Mauldin, R. L., Baalbaki, R., Brilke, S., Dada, L., Dias, A., Duplissy, J., El Haddad, I., Finkenzeller, H., Fischer, L., He, X., Kim, C., Kürten, A., Lamkaddam, H., Lee, C. P., Lehtipalo, K., Leiminger, M., Manninen, H. E., Marten, R., Mentler, B., Partoll, E., Petäjä, T., Rissanen, M., Schobesberger, S., Schuchmann, S., Simon, M., Tham, Y. J., Vazquez-Pufleau, M., Wagner, A. C., Wang, Y., Wu, Y., Xiao, M., Baltensperger, U., Curtius, J., Flagan, R., Kirkby, J., Kulmala, M., Volkamer, R., Winkler, P. M., Worsnop, D., and Donahue, N. M.: Molecular Composition and Volatility of Nucleated Particles from á-Pinene

Oxidation between −50 °C and +25 °C, Environ. Sci. Technol., 53, 12357–12365, https://doi.org/10.1021/acs.est.9b03265, 2019.

Yue, M., Dong, X., Wang, M., Emmons, L. K., Liang, Y., Tong, D., Liu, Y., and Liu, Y.: Modeling the Air Pollution and Aerosol-PBL Interactions Over China Using a Variable-Resolution Global Model, J. Geophys. Res.-Atmos., 128, e2023JD039130, https://doi.org/10.1029/2023jd039130, 2023.

Zaveri, R. A., Easter, R. C., Singh, B., Wang, H., Lu, Z., Tilmes, S., Emmons, L. K., Vitt, F., Zhang, R., Liu, X., Ghan, S. J., and Rasch, P. J.: Development and Evaluation of Chemistry-Aerosol-Climate Model CAM5-Chem-MAM7-MOSAIC: Global Atmospheric Distribution and Radiative Effects of Nitrate Aerosol, J. Adv. Model. Earth Sy., 13, e2020MS002346, https://doi.org/10.1029/2020MS002346, 2021.

Zawadowicz, M. A., Lee, B. H., Shrivastava, M., Zelenyuk, A., Zaveri, R. A., Flynn, C., Thornton, J. A., and Shilling, J. E.: Photolysis Controls Atmospheric Budgets of Biogenic Secondary Organic Aerosol, Environ. Sci. Technol., 54, 3861–3870, https://doi.org/10.1021/acs.est.9b07051, 2020.

Zhang, Y. M., Zhang, X. Y., Sun, J. Y., Lin, W. L., Gong, S. L., Shen, X. J., and Yang, S.: Characterization of new particle and secondary aerosol formation during summertime in Beijing, China, Tellus B, 63, 382–394, https://doi.org/10.1111/j.1600-0889.2011.00533.x, 2011.

Zhao, D., Schmitt, S. H., Wang, M., Acir, I.-H., Tillmann, R., Tan, Z., Novelli, A., Fuchs, H., Pullinen, I., Wegener, R., Rohrer, F., Wildt, J., Kiendler-Scharr, A., Wahner, A., and Mentel, T. F.: Effects of NO_x and SO_2 on the secondary organic aerosol formation from photooxidation of α-pinene and limonene, Atmos. Chem. Phys., 18, 1611–1628, https://doi.org/10.5194/acp-18-1611-2018, 2018.

Zheng, J., Zhang, L., Che, W., Zheng, Z., and Yin, S.: A highly resolved temporal and spatial air pollutant emission inventory for the Pearl River Delta region, China and its uncertainty assessment, Atmos. Environ., 43, 5112–5122, https://doi.org/10.1016/j.atmosenv.2009.04.060, 2009.

Zhou, Y., Zhao, Y., Mao, P., Zhang, Q., Zhang, J., Qiu, L., and Yang, Y.: Development of a high-resolution emission inventory and its evaluation and application through air quality modeling for Jiangsu Province, China, Atmos. Chem. Phys., 17, 211–233, https://doi.org/10.5194/acp-17-211-2017, 2017.

Zhu, J. and Penner, J. E.: Global Modeling of Secondary Organic Aerosol With Organic Nucleation, J. Geophys. Res.-Atmos., 124, 8260–8286, https://doi.org/10.1029/2019jd030414, 2019.

Zhu, J. L., Penner, J. E., Yu, F. Q., Sillman, S., Andreae, M. O., and Coe, H.: qjDecrease in radiative forcing by organic aerosol nucleation, climate, and land use change, Nat. Commun., 10, 423, https://doi.org/10.1038/s41467-019-08407-7, 2019.